Sensitivity Testing of WRF Physics Parameterizations for Meteorological Modeling and Protocol in Support of Regional SIP Air Quality Modeling in the OTR

Ozone Transport Commission

Modeling Committee

Editor: Debra Baker MDE

Contributors

Debra Baker MDE

Tom Downs ME DEP

Mike Ku NYS DEC

Winston Hao NYS DEC

Gopal Sistla NYS DEC

Mike Kiss VA DEQ

Matt Johnson IA DNR

David Brown IA DNR

Table of Contents

1. Introduction

This document describes the preparation of the mesoscale meteorological model fields that will be used for air quality modeling in support of State Implementation Plans (SIPs) in the Ozone Transport Region (OTR). The OTR includes Connecticut, Delaware, the District of Columbia, Maine, Maryland, Massachusetts, New Hampshire, New Jersey, New York, Pennsylvania, Rhode Island, Vermont, and portions of NorthernVirginia.

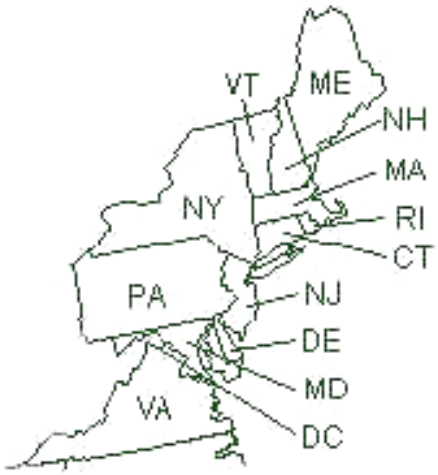

The United States Environmental Protection Agency (EPA) recommends that a modeling protocol be developed to reflect consensus among various organizations on the methods and procedures to be followed. [40 CFR § 51, App. W, 10.2.1(a)]. To meet this requirement, portions of this protocol were prepared in collaboration with a specially-formed "WRF Work Group". Its members included the Mid-Atlantic/Northeast Visibility Union (MANE-VU: which includes the OTC), Lake Michigan Air Directors Consortium (LADCO), the Southeastern States Air Resource Managers Inc. (SESARM), and the State of Iowa.

Consensus was reached on the mesoscale model, domain, vertical layers, and some of the physics parameterization options. Ultimately, regional differences warranted the use of slightly different parameterizations but all participants agreed that the meteorology fields prepared would be shared among all groups.

The purpose of this protocol is to summarize the modeling activities required to support the development of the 2007 meteorological data . These activities include:

- Selection and description of the modeling system;
- Modeling episodes, extent and resolution of the three-dimensional grid;
- Selection of appropriate databases and modeling episodes;
- Establishing performance benchmark, model configuration sensitivity simulations;
- Final model configuration and operational testing of the meteorological model;
- Performance evaluation methodology;
- Delivery of the meteorological model outputs for subsequent use in air quality modeling;
- Documentation of the meteorological modeling study findings.

This document benefits from EPA guidance on regulatory modeling, published scientific literature, and modeling experience of staff at various regulatory agencies involved in this process.

The goal is to create scientifically reliable simulations of atmospheric dynamics observed over the Eastern United States. The simulated fields will be used for air quality modeling to determine the effectiveness of emission control strategies in attaining the ozone and $PM_{2.5}$ National Ambient Air Quality Standards (NAAQS) and meeting the Regional Haze visibility goals. A detailed listing of legal and regulatory SIP obligations is provided in Appendix A of this protocol. The OTC concurrently addressed these requirements using a single integrated, one-atmosphere air quality modeling platform because similar pollutants, emissions, and atmospheric processes control chemical formation and transport for fine particles, ozone, and regional haze. Model Selection
The meteorology model is a critical component of air quality simulations. According to *Gilliam et al.* (2009), high quality meteorology inputs are necessary for "accurate representations of air flow and dispersion, cloud properties, radiative fluxes, temperature and humidity fields, boundary layer evolution, and surface fluxes of both meteorological quantities (heat, moisture, and momentum) and chemical species (dry deposition)."

Air quality agencies have traditionally utilized the Pennsylvania State University / National Center for Atmospheric Research mesoscale model (MM5) to produce meteorological fields for photochemical modeling. However, the mesoscale meteorology model used for operational weather forecasts has now shifted to the Weather Research and Forecasting (WRF) model. WRF has been a collaborative partnership, principally among the National Center for Atmospheric Research (NCAR), National Oceanic and Atmospheric Administration (NOAA), National Centers for Environmental Prediction (NCEP) and Forecast Systems Laboratory (FSL), Air Force Weather Agency (AFWA), the Naval Research Laboratory (NRL), University of Oklahoma, and the Federal Aviation Administration (FAA). MM5 is no longer being updated so WRF represents the

current state of the science. WRF also includes improvements including mass conservation, updated dynamics, and new physics parameterizations.

WRF was selected for use in upcoming SIP air quality modeling by a consensus of several RPOs because the model is:

- Generally considered the most technically advanced public-domain prognostic model available for operational use in preparing inputs to urban- and regional-scale photochemical air quality models.
- Suitable for a broad spectrum of applications across scales ranging from meters to thousands of kilometers.
- Flexible and efficient computationally, while offering the advances in physics, numerics, and data assimilation contributed by the research community.

In addition, EPA expects that air quality modelers will also shift from MM5 to WRF (http://www.epa.gov/scram001/metmodel.htm).

Several research studies have compared the performance of MM5 and WRF. *Lin et al*. (2006) found that WRF was better as input to Models-3/Community Multiscale Air Quality model (CMAQ) than MM5 after comparing ozone concentrations to observations. In particular, WRF was better at reproducing the magnitude and spatial variation of rainfall.

Appel et al. (2009) did a thorough performance comparison of WRF and MM5 meteorology fields by comparing CMAQ results for the Eastern United States using both types of input. They compared a winter month (January 2006) and summer month (August 2006) and examined both ozone and $PM_{2.5}$ concentrations produced by CMAQ.

They found that WRF has similar performance for 2 m temperature as MM5, but WRF had a lower bias in winter during nighttime. For 2 m water vapor mixing ratio, WRF has a significant reduction in bias in summer during daytime. MM5 has a lower bias for 10 m wind speed in the winter. Both WRF and MM5 overpredicted precipitation but WRF has a smaller overprediction than MM5 for summer convective precipitation. WRF also has a lower bias and smaller error for wet deposition. WRF has a slightly higher bias for ozone and $PM_{2.5}$ in both seasons but better performance for nitrates and similar performance for total carbon. The differences between the models were due to different formulas for friction velocity, predicted cloud cover, vegetation fraction, leaf area index, and convective precipitation. Overall, *Appel et al.* concluded that the WRF model is generally performing in a manner comparable to the MM5 for the meteorological variables required by CMAQ.

Gilliam et al. (2009) found that WRF is comparable or better than MM5 in error statistics for 2-m temperature, 2-m water vapor mixing ratio, and 10-m wind as long as objective analysis (OBSGRID) and four-dimensional data assimilation (FDDA) are used. They found that WRF temperature in planetary boundary layer (PBL) had a median absolute error of 1.0 to 1.5 K or less. They also found that WRF wind speed profile had a low error of less than 2.0 m s^{-1} and was able to accurately recreate nocturnal low level jets (NLLJ) and the convective mixed layer.

In *de Meij et al.* (2009), researchers compared WRF to MM5 as input for another chemical transport model (CHIMERE). The biggest differences were in PBL height: at noon in January, WRF PBL height was 2.8 times higher than MM5. WRF did a better job of simulating the hourly diurnal changes in relative humidity. For winter simulations, they found that rain was overestimated by WRF but underestimated by MM5. The hit rate scores for WRF were generally better in winter. For summer, WRF catches the precipitation events better than MM5. In the winter and summer, MM5 and WRF underestimated relative humidity, but MM5 had the larger root mean square error (RMSE) and smaller correlation values. While both models overestimated wind speed, WRF had lower RMSE in winter and similar performance in summer. Wind direction accuracy was comparable for both models: good in winter and poor in summer. Both underestimated temperatures, but WRF had lower errors in the winter and similar results in the summer. WRF outperformed MM5 for potential temperature gradient profiles from soundings.

Gilliam and Pleim (2010) concluded that "WRF performance is now at or above the level of MM5 [and] is thus recommended to drive future air quality applications."

2. Model Description

The WRF v. 3.1 mesoscale meteorology model is a fully compressible, nonhydrostatic model with an Eulerian mass dynamical core [*Skamarock et al*. 2008]. Two dynamical cores are available: the Advanced Research WRF (ARW) core, developed and supported by NCAR, and the Nonhydrostatic Mesoscale Model (NMM) core, whose development is centered at NCEP's Environmental Modeling Center (EMC) and support is provided by NCAR's Development Testbed Center (DTC). The WRF-NMM is designed to be a real-time forecast model so physics schemes are preset. The OTC chose WRF-ARW (hereinafter WRF) because it includes multiple physics options for turbulence/diffusion, radiation (long and shortwave), land surface, surface layer, planetary boundary layer, cumulus, and microphysics.

Time integration is performed with a 3rd-order Runge-Kutta scheme. WRF has split time integration, which uses smaller time steps used for fast processes like sound waves or gravity waves. WRF was designed to conserve mass, momentum, entropy, and scalars using flux form prognostic equations.

WRF uses Eta (η) as a vertical coordinate, which is defined as the hydrostatic pressure difference from the layer to the top divided by the difference in the entire vertical domain so it is always between 1 (surface) and 0 (top). This vertical coordinate is terrain following hydrostatic pressure system.

The grid format is Arakawa- C with all variables in the center of the grid except for wind velocity which is defined on the edges of the grid, and shared between adjacent grids.

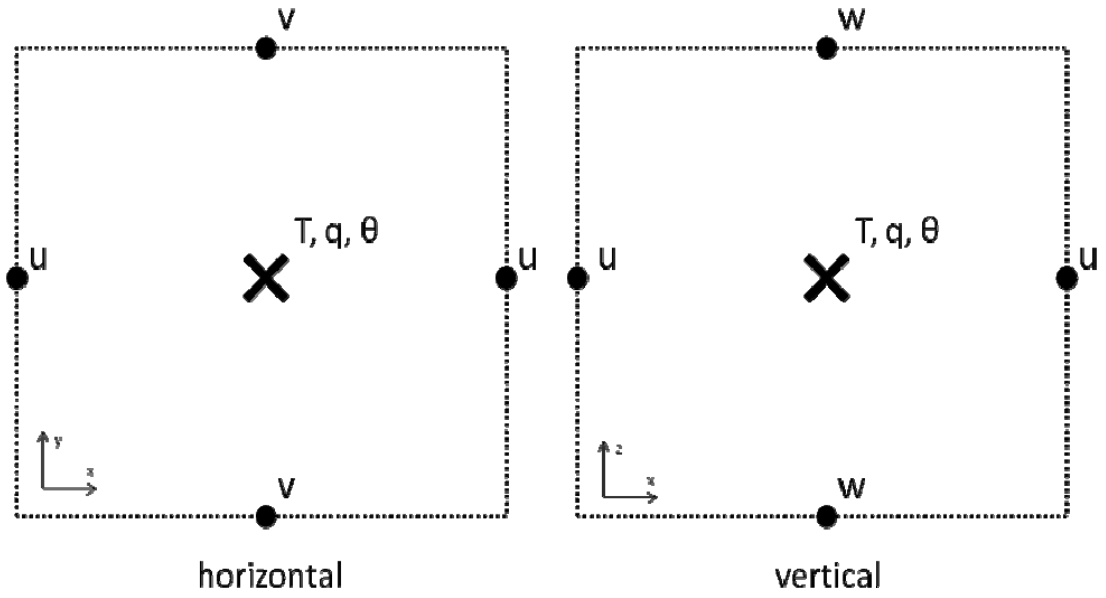

The WRF core uses a 3rd-order Runge-Kutta split-explicit time integration scheme, high-order advection scheme, and is scalar conserving. It contains complete Coriolis, curvature, and mapping terms. Domain nesting is possible with one-way and two-way capabilities. Full physics options are available to represent atmospheric radiation, surface and boundary layers, and cloud and precipitation processes. The model contains gridded analysis and observational nudging four dimensional data assimilation (FDDA) capabilities that allow users to perform enhanced retrospective analyses.

The WRF modeling system is divided into two main components: the WRF Preprocessing System (WPS) and the WRF modeling core. WPS contains three processors that define the WRF modeling domain, generate map, elevation/terrain, and land-use data, and generate horizontally interpolated input meteorological fields to the WRF grid. The WRF modeling core interpolates the meteorological fields processed by WPS to the WRF vertical levels and generates initial and lateral boundary conditions. The model solver integrates the atmospheric equations and interfaces with the physics parameterizations to generate forecasts of meteorological variables.

WRF uses physics sub-models to simulate land surface, surface layer, and boundary layer dynamics, along with cumulus convection, microphysics, and radiation. For each of these sub-models, WRF offers from 3 to 9 different parameterizations from which the modeler may select. To make these choices, the modeler must consider not only the individual merits of each parameterization but also how it interacts with the other physics sub-model options. The following flow chart illustrated the interaction of the WRF physics sub-modules.

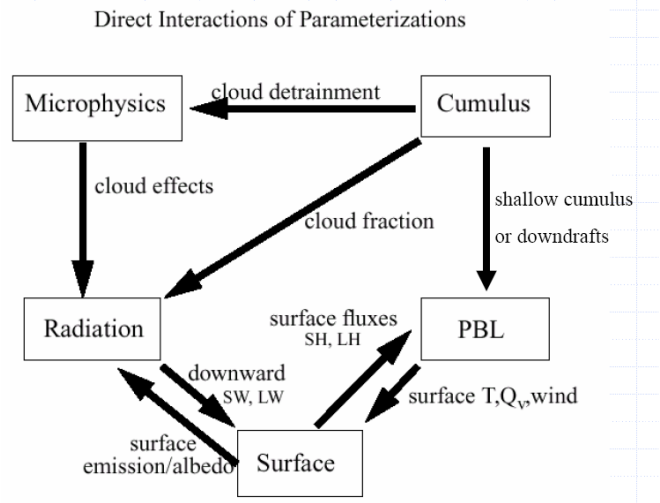

The latest release of WRF is version 3.1.1 (July 2009), would be utilized in this exercise. The main update to the model in this release was the addition of objective analysis (OBSGRID) and surface analysis nudging capabilities, an option preferred for generating meteorological data for input to air quality simulations.

3. Time Period

The OTC Modeling Committee reached a consensus for developing the meteorological data that would be common and satisfies the needs to address both the 8-hr ozone and 24-hr $PM_{2.5}$ attainment in the OTR. As part of this effort, the selected period, in this case should be of recent vintage to reflect the development of emissions inventories as well as meteorologically conducive for both ozone and $PM_{2.5}$ events.

With these requirements, the measured air pollutant data for 2005 through 2009 were examined over the OTR as well as the upwind regions of interest. Tom Downs of ME DEP was instrumental in developing the analytical framework and complete analysis is available at http://www.maine.gov/dep/ftp/OTC_MOD_COM/

In this Section, a brief synopsis of these analyses is provided.
The EPA modeling guidance on Demonstrating Air Quality Goals for Ozone, $PM_{2.5}$, and Regional Haze identified the following criteria for selecting episodes suggesting that at a minimum, four criteria should be used to select time periods which are appropriate to model:

1) Simulate a variety of meteorological conditions:

a) 8-Hour Ozone- Choose time periods which reflect a variety of meteorological conditions which frequently correspond with observed 8-hour daily maxima $\geq$ 75 ppb at multiple monitoring sites.

b) 24-Hour $PM_{2.5}$ - Choose time periods which reflect a variety of meteorological conditions which frequently correspond with observed 24-hour averages $\geq 35\ \mu g/m^3$ at violating monitoring sites.

c) Annual $PM_{2.5}$ - Choose time periods from each quarter which reflect the variety of meteorological conditions which represent average concentrations for that quarter and year

d) Regional Haze- .Choose time periods which reflect the variety of meteorological conditions which represent visibility impairment on the 20% best and 20% worst days in the Class I areas being modeled.

2) Model time periods in which observed concentrations are close to the appropriate baseline design value or visibility impairment.

3) Model periods for which extensive air quality/meteorological data bases exist.

4) Model a sufficient number of days so that the modeled attainment test applied at each monitor violating the NAAQS is based on multiple days.

Following this guidance, measured air quality and meteorological data were assembled for 2002 to 2008 and analyzed to identify the appropriate year for use in the OTC Modeling effort.

For the 24-hr $PM_{2.5}$, monitors violating the NAAQS of 35μg/m^3 were identified across the OTR and grouped by season as the modeling guidance requires assessment of each quarter in developing the attainment demonstration. Both 2005 and 2007 were found to be candidates with design values in the range of 36 to 43μg/m^3 except for one location at 60μg/m^3 in the western portion of the OTR.

In the case of 8-hr ozone, the measured data over the OTR were analyzed focus was on 24-hr NAAQS which is the 98th percentile of the daily average concentration over the OTR and Upwind regions for the period of 2002 to 2008. The 2007 design values for 8-hr ozone were in the range of 76 to 92 ppb. Recently the EPA revised the methodology for estimating design value concentrations as well as is in the process of promulgating new 8-hr ozone NAAQS as well as a secondary NAAQS that differs from the existing one. This analysis has not addressed these issues, but reflects the 8-hr ozone NAAS of 75 ppb. Based upon these analyses, and the need to have the base year for modeling not far removed from the State Implementation Plan (SIP) inventory year, which in this case was 2008, the OTC Modeling Committee reached the consensus and selected 2007 as the modeling base year.

4. Modeling Domain

The domain used by the OTC has been expanded from the domain used for the 2002 State Implementation Plan modeling. This was done to coordinate with the other members of the WRF Work Group, which including LADCO, SESARM, and the State of Iowa.

4.1. Horizontal Grid

The computational domain for this simulation consists of a coarse and fine grid nested domains. The coarse domain consists of a Lambert conic conformal projection with specifications used in previous regional modeling studies, which is centered at 40° N and 97° W with true latitudes of 33 and 45° N. The coarse grid structure consists of an array of 165 cells in the east-west direction and 129 cells in the north-south direction with a grid spacing of 36 kilometers (km). This domain was designed maximize the usage of the Eta analysis region.

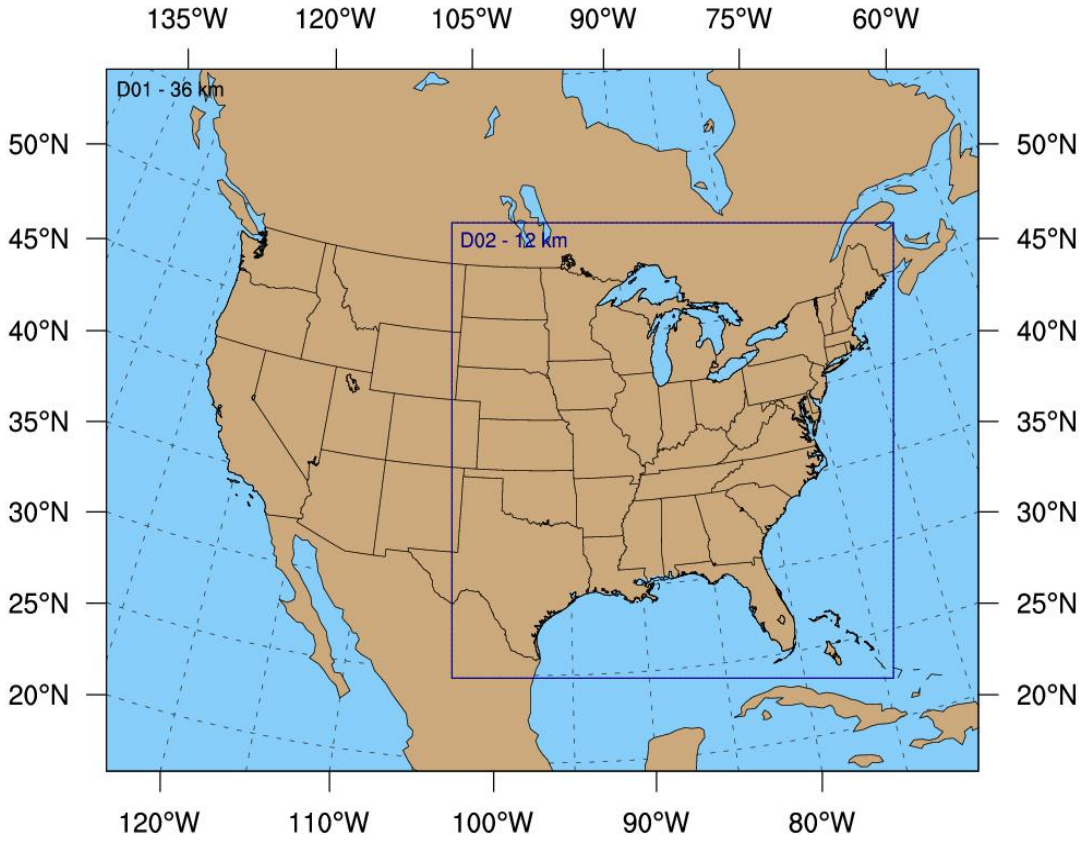

A nested domain is implemented to resolve finer scale meteorological features. The nested domain grid structure is a 250 by 250 array of grid cells with a grid spacing of 12 km. This domain begins at node (66, 18) of the course domain. The nested domain shares the northern, eastern, and southern boundaries of the EPA 12 km Eastern domain

and western boundary of the Iowa/LADCO 12 km domain. A summary of the horizontal structure of the modeling domain is given in Table below.

Domains	Outer (1)	Inner (2)
Resolution (km)	36	12
Starting Location (i,j)	1,1	66,18
nx (E-W)	165	250
ny (N-S)	129	250
SW Coordinate (km)	-2952, -2304	-612, -1692
NE Coordinate (km)	2952, 2304	2376, 1296

Using 12 km horizontal resolution is sufficiently high to simulate mesoscale features and is also in range to use both WRF microphysics and cumulus convection schemes.

The option of using 12 km resolution for the entire domain rather than doing a nested simulation was discussed in the WRF Coordination Committee. The OTC agreed with other regions that a 36-km outer domain allowed for initial screening to be run more quickly by the use of a lower resolution, and the computational overhead will be minimized.

The input file used by the WRF Preprocessor System to create the model domain is provided in Appendix B.

4.2. Vertical Layers

The vertical grid structure consists of 35 layers as shown below.

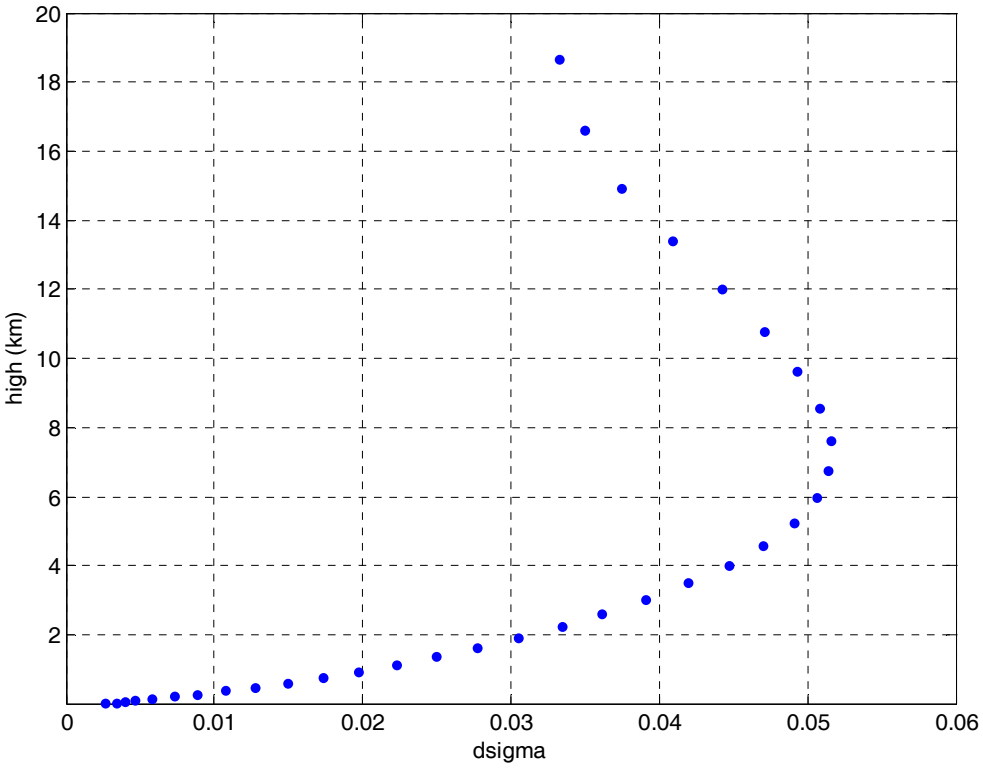

This vertical structure was designed to provide increased resolution in the boundary layer and near the tropopause. The second level is placed at ~20 meters so that the midpoint of the grid cells in the vertical direction is located at 10 meters and corresponds to the standard National Weather Service (NWS) anemometer height. This avoids the use of a surface layer parameterization to vertically interpolate horizontal wind components to the standard NWS observational height. The top of the model is fixed at 50 millibars (mb). A summary of the vertical structure of the modeling domain is given in Table below.

Level	Sigma	Height (m)	Pressure (mb)	Depth (m)
35	0.0000	18663	50	2034
34	0.0332	16629	82	1715
33	0.0682	14914	115	1515
32	0.1056	13399	150	1375
31	0.1465	12024	189	1255
30	0.1907	10769	231	1145
29	0.2378	9624	276	1045
28	0.2871	8579	323	955
27	0.3379	7624	371	870
26	0.3895	6754	420	790
25	0.4409	5964	469	715
24	0.4915	5249	517	645

Level	Sigma	Height (m)	Pressure (mb)	Depth (m)
23	0.5406	4604	564	580
22	0.5876	4024	608	520
21	0.6323	3504	651	465
20	0.6742	3039	690	415
19	0.7133	2624	728	370
18	0.7494	2254	762	330
17	0.7828	1924	794	293
16	0.8133	1631	823	259
15	0.8410	1372	849	228
14	0.8659	1144	873	200
13	0.8882	944	894	174
12	0.9079	770	913	150
11	0.9252	620	929	128
10	0.9401	492	943	108
9	0.9528	384	955	90
8	0.9635	294	965	74
7	0.9723	220	974	60
6	0.9796	160	981	48
5	0.9854	112	986	38
4	0.9900	74	991	30
3	0.9940	44	994	24
2	0.9974	20	998	20
1	1.0000	0	1000	0

The input file used by the WRF to create the vertical domain is provided in Appendix B.

An initial sensitivity test was run in which the second level was set at ~10 m instead of ~20 m. This change slightly improved nighttime low wind speeds but had significantly degraded the daytime peak wind speeds. It did not affect temperature but moved the humidity peak from the afternoon to late morning with no increase in accuracy. Based on these results, the ~20 m height was selected for the WRF simulations.

5. Input Data and Modeling

5.1. The WRF model requires input of initial and boundary conditions, land use and topography data. Initial and Boundary Conditions

The initial and boundary conditions for the WRF model will be obtained from the NCEP North American Mesoscale (NAM) analysis datasets. Some of these data are from the operational run of the Weather Research and Forecasting - Nonhydrostatic Mesoscale Model (WRF-NMM), which replaced the Eta mode on June 20, 2006. These data are in 40-km resolution. The domain is NCEP Grid 212, which covers the contiguous United States as well as most of Canada and Mexico.

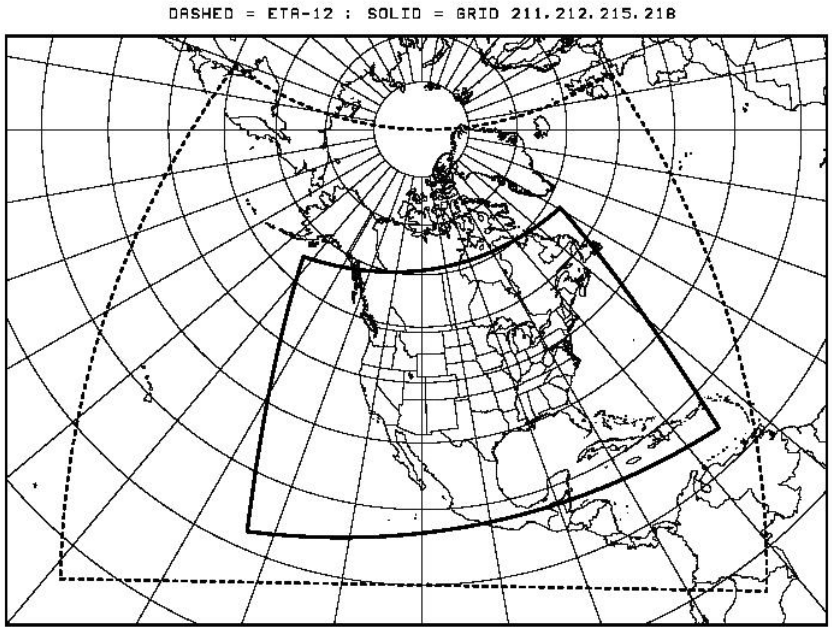

The domain uses a Lambert Conformal Conic (LCC) map projection and has 185 x 129 grid squares. The EDAS/NDAS 3D and surface analysis fields are available every 3 hours from NCAR in their Computational and Information Systems Laboratory (CISL) Research Data Archive (NCAR archive, http://dss.ucar.edu/datasets/ds609.2/). The model dataset has the following data assimilated:

- Rawinsonde pressure, temperature and wind;
- Piball winds;
- Dropwindsondes;
- Wind profiles;
- Surface land temperature and moisture;
- Oceanic surface data (ship and buoys);
- Aircraft winds;

- Satellite cloud-drift winds;
- Oceanic TOVS thickness retrievals; and
- GOES and SSM/I precipitable water retrievals.

5.2. Geography Files

The OTC initialized WRF with static data for topography, land use, and soil types for the bottom and top layers. This data was in 10 minute resolution for the outer domain and 2 minute resolution for the inner nest. There are 16 soil categories.

Code	Soil Category
1	Sand
2	Loamy sand
3	Sandy loam
4	Silt loam
5	Silt
6	Loam
7	Sandy clay loam
8	Silty clay loam
9	Clay loam
10	Sandy clay
11	Silty clay
12	Clay loam
13	Organic matter
14	Water
15	Bedrock
16	Other

The United States Geological Survey (USGS) 24 land use categories were used.

Code	Land Use Category
1	Urban
2	Dryland crop pasture
3	Irrigated crop pasture
4	Mixed crop pasture
5	Cropland and grassland
6	Cropland and woodland
7	Grassland
8	Shrubland
9	Shrubland and grassland
10	Savanna
11	Deciduous broadleaf
12	Deciduous needleleaf
13	Evergreen broadleaf
14	Evergreen needleleaf
15	Mixed forest
16	Water bodies
17	Herbaceous wetland
18	Wooded wetland
19	Barren or sparse vegetation
20	Herbaceous tundra
21	Wooded tundra
22	Mixed tundra
23	Bare ground tundra
24	Snow and ice

Other static fields provided by the WRF Preprocessing System geographical files were soil temperature, green fraction, and snow albedo.

5.3. Data Nudging

To minimize the accumulation of model errors and retain as many mesoscale circulations as possible, the Objective Analysis and Four-Dimensional Data Assimilation (FDDA) techniques will be used to include observations of the surface winds and upper-level meteorological information. The datasets used are high resolution (in time and space) and the technique has been applied in previous air quality modeling studies. *Gilliam et al.* (2009) found big improvements in WRF results when OBSGRID, was used to lower error of analyses.

5.3.1. Objective Analysis

The OBSGRID option, just introduced in WRF v. 3.1, is used for objective analysis. The goal of OBSGRID is to improve the first-guess gridded analysis by incorporating high-resolution observations with the low-resolution global analysis [*Wang et al.* 2009]. It produces improved initial and boundary input files for WRF.

The Cressman style objective analysis was used, in which several successive scans nudge a "first-guess" field toward each neighboring observed value within a circular radius of influence from each grid point. A distance-weighted average of the difference between the "first guess" and the observations is added to the value of the "first guess" at each grid point. Once all grid points have been adjusted, the adjusted field is used as the "first guess" for another adjustment cycle with a smaller radius of influence.

5.3.2. Four-Dimensional Data Assimilation

In contrast to objective analysis, which is used to improve initial and boundary conditions, FDDA incorporates observations during model integration [*Stauffer et al.* 1991]. The FDDA options chosen for the OTC WRF runs were analysis and surface nudging. The surface FDDA option creates a separate surface analysis that has a higher temporal resolution than full 3D analyses. The analysis nudging uses 3D gridded variables above the surface layer that are used throughout the WRF run to nudge model outputs toward the analysis, which is based on observations [*Wang et al.* 2009].

The input data was set at 3-hour intervals and ran for 5 hours and 10 minutes during each segment. In the boundary layer, only U and V winds were nudged (Note that the 10-m wind is a diagnosed variable and is not directly nudged). Nudging of temperature at the surface was not used because it can cause static instability if it is not consistent with temperature above the surface layer [*Stauffer et al.* 1991]. The water vapor mixing ratio is also not nudged in the PBL because supersaturation may occur when surface temperature is not nudged. In the free troposphere, nudging was used for U and V winds, temperature, and water vapor mixing ratio to help minimize large-scale errors.

5.3.3. Nudging Coefficients

The strength of dynamical nudging depends on the magnitude of the nudging coefficients selected. The nudging coefficient for wind should not exceed that of the Coriolis parameter in the PBL, where three-way balance with pressure gradient and fiction force holds [*Gupta et al.* 1997]. The nudging coefficients used for the OTC WRF runs are listed below.

Domain	Variable Nudged	Nudging Coefficient
Outer Domain	U and V winds	5.0×10^{-4}
Outer Domain	Temperature	5.0×10^{-4}
Outer Domain	Water vapor mixing ratio	1.0×10^{-5}
Inner Nest	U and V winds	2.5×10^{-4}
Inner Nest	Temperature	2.5×10^{-4}
Inner Nest	Water vapor mixing ratio	1.0×10^{-5}

The inner nest nudging coefficients are similar to those used in air quality retrospective studies. *Gupta et al.* (1997) tested various nudging coefficients for wind and found that 2.778×10^{-4} best replicated the energy spectrum. *Mao et al.* (2006) used 2.5×10^{-4} for temperature and wind and 1.0×10^{-5} for water vapor mixing ratio. *Gilliam and Pleim*

(2010) used a slightly higher nudging coefficient for temperature and wind (3.0×10^{-4}) but the same for moisture (1.0×10^{-5}).

The outer domain nudging coefficients were determined after testing at different levels. Using lower coefficients, the OTC found that the 3D analysis and surface nudging had very little impact on surface and upper air variables. As a result, higher settings were chosen for the outer domain to improve WRF performance.

5.3.4. Surface and Analysis Datasets

NCEP's ADP global surface wind observations (NCAR archive ds461.0) are used for FDDA. This dataset includes land and marine surface reports received via the Global Telecommunications System (GTS). Variables recorded in the reports include pressure, air temperature, dewpoint temperature, wind direction, and wind speed. Precipitation data has been decoded for the U.S. and Canada. Report intervals range from hourly to 3 hourly. These data are the primary input to the NCEP Global Data Assimilation System (GDAS). In addition, NCEP's ADP global upper-air observations (NCAR archive ds351.0) are used to enhance the upper-level analysis.

5.3.5. Data Screening

The OTC WRF runs also used several OBSGRID algorithms to screen for suspect data in the analysis. First, Quality Control was used to remove spikes from temperature and wind profiles and to adjust temperature profiles to remove superadiabiatic layers. The ERRMAX test and Buddy Test were also applied. For the ERRMAX Test, the user sets thresholds to vary the tolerance of the error check. These thresholds vary depending on the field, level, and time of day. If the difference between the observation and the "first guess" exceeds the threshold, the observation is discarded. For the Buddy test, the user sets weighting factors to vary the tolerance of the error check. If the difference between an observation and the "first guess" varies significantly from the distance-weighted average of this difference for neighboring observations, the observation is discarded. These two tests are both highly recommended for simulations with OBSGRID [*Wang et al.* 2009]. In addition, the OBSGRID was modified to include wind speed less than 0.1meter/sec.

6.4 Annual Model Simulation

The WRF model integrations will be re-initialized every 5.5 days, allowing a 12-hour period for the model spin-up (i.e., the first 12 hours of data were discarded in the application of the datasets).

6.5 Benchmark Simulations

The benchmark run was set to test that each modeling center with different computer platform/compiler would generate the same results by running the model with same inputs and physics options. A five and half day period in the summer of 2007 was selected and UMD prepared the inputs and posted on the UMD's FTP site for access by each modeling center use. NYSDEC analyzed and compared the benchmark simulations

and found significant differences in results between the modeling centers, even when the same compiler was used.

WRF developers were notified on the problem of inconsistencies of WRF simulation between modeling centers, and there were going to be delays to rectify the problem . Rather than to wait for resolving the hardware/compiler issues, it was decided that a static compiled version (prepared by UMD) to be used by all modeling centers.

7. Sensitivity Testing

One of the goals of the sensitivity testing was to establish a set of parameters that would provide what is considered as comparatively a better or best simulation of the limited observed meteorological fields, since WRF is exercised in a prognostic or non-forecasting mode. The methodology that was adopted was to exercise the model for two periods – one summer and one winter – with different configurations and to examine the simulated fields to measured data.

7.1 Model Setup and Assessment

Under the benchmark exercise, it was determined that a pre-compiled static-executable code would be used in this study. This step enables each of the modeling Centers to complete a set of simulations and provide results for assessment rather than one modeling Center performing all the runs, thus accelerating the process. It was also agreed that the input data would be prepared and distributed by Prof. Dalin Zhang and his students of the University of Maryland (UMD) thereby providing a common basis for any changes in the input data.

All sensitivity runs were performed for the 20-day summer period (July 28 to August 15, 2007) and the 20-day winter period (December 5 to 24, 2007). These dates were chosen by the WRF Work Group based on known air quality exceedances throughout the Eastern United States. In each seasonal assessment WRF results were examined in terms of daily (24 hours), daytime (15z to 20z), and nighttime categories (03z to 08z). Note that daytime and nighttime comprise only 6 hours each so that transition times could be excluded.

Two observation databases were used for model performance assessment. The first was Technical Development Laboratory (TDL) observations based on the Automated Surface Observing Systems (ASOS) maintained by NWS. The second set of observations is from the Clean Air Status and Trends Network (CASTNet), based on meteorological instruments co-located with air quality monitors. CASTNet sites are located in rural areas and sensitive ecosystems. While the WRF Work Group reviewed results for each region in the Eastern U.S., this summary will focus on the results for the OTC states.

The classic approach for model evaluation was used for assessing the sensitivity of WRF parameterizations: to compare observations with model results. Domain-wide statistics are used as a measure of general performance [*Borge et al.* (2008)]. As in many studies

[*e.g.*, *Appel, et al*. 2009; *Gilliam & Pleim* 2010], the primary variables for evaluation were 2 m temperature, 2 m water vapor mixing ratio, and 10 m wind speed and direction.. The spatial and temporal distribution of precipitation plays a key role in atmospheric chemistry so it was also evaluated. In addition, upper air performance was evaluation by using vertical soundings, wind profilers, and satellite cloud data. The statistical tests chosen for the assessment were the root-mean square error (RMSE) and correlation coefficient (CORR). The daily RMSE and CORR were calculated and compared. This will provide information to determine a configuration in general with better performance in various meteorological conditions.

7.2 PBL Schemes

The majority of the WRF sensitivity runs were done to compare planetary boundary layer (PBL) schemes. This parameterization is crucial to air quality studies because it determines the near-surface temperature, which significantly affects ozone production, the near-surface moisture, which significantly affects $PM_{2.5}$, and near-surface winds, which significantly affects dispersion and local transport.

Many studies have shown that accurately simulating PBL dynamics is the most critical aspect of meteorology physics for air quality modeling. For example, *Lin et al.* (2009) noted the "important role of diurnal boundary layer fluctuations in controlling ground-level O_3." They found that vertical mixing, urban chemistry, and dry deposition depending on PBL height strongly affected CMAQ's ability to capture observed ozone concentrations. If PBL heights are too low, they found that CMAQ had too much ozone build-up near the ground during the day and too much NO_x titration at night.

The sensitivity tests initially looked at four PBL schemes that have been included in the WRF package. The Mellor, Yamada, and Janjiç scheme (MYJ and Yonsei University schemes (YSU) both had been widely used in the weather forecast community that is more interesting in the upper air pattern that drives the weather system. For the air quality modeling, it is crucial in accurately simulating near surface variables, such as wind field and mixing ratio. The Asymmetric Convective Model version 2 (ACM2 PX) developed by Pleim and Xiu of USEPA had been used extensively in CMAQ modeling for ozone and $PM_{2.5}$, and now is also available in the WRF system. Another PBL scheme selected for the sensitivity testing is modified Blackadar scheme (BLK) developed by Professor Zhang of UMD. BLK scheme had been used successfully in 2002 MM5 simulations for OTC SIP modeling. Professor Zhang had made effort to adapt BLK into WRF and submitted to NCAR WRF developers for review and to be included in the official WRF release. In all, four PBL parameterizations were selected for WRF sensitivity testing.

Name	Abbrev.	Description
Mellor, Yamada, and Janjiç	MYJ	Eta operational scheme. One-dimensional prognostic turbulent kinetic energy scheme with local vertical mixing
Yonsei University	YSU	Eddy diffusion K scheme with explicit entrainment layer and parabolic K profile in

Name	Abbrev.	Description
		unstable mixed layer
Pleim-Xiu Asymmetric Convective Model 2	ACM2(PX)	Asymmetric nonlocal scheme. Non-local upward mixing and local downward mixing with an eddy diffusion algorithm. New in WRF v. 3.0
Modified Blackadar	BLK	Symmetric nonlocal scheme. Determines the K-coefficient by the Richardson number and mixing length is first model layer thickness (MM5 scheme adapted for WRF by UMD)

These PBL schemes were tested with several microphysics, land surface, and surface layer schemes, which will be presented in § 7.3 below. For comparability, the statistics presented in this section will show the MYJ, YSU, and BLK results using WSM6 microphysics and the NOAH land model. The ACM2 results also used WSM6 microphysics along with the Pleim-Xiu land model (PX LSM).

7.2.1 Temperature

Observations of 2 m temperature were compared with the results of each PBL scheme for both summer and winter periods. The New York modeling center created time series correlation plots for summer 2 m temperature in the MANE-VU region divided into daily, daytime, and nighttime.

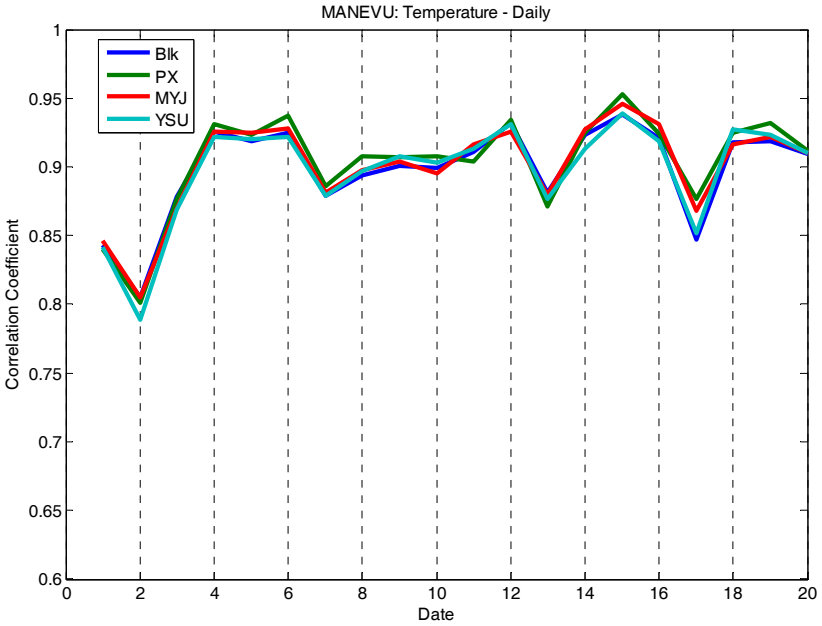

For the summer, the ACM2 (PX) scheme did better than the other PBL schemes, but differences among the parameterizations was only 1–2%.

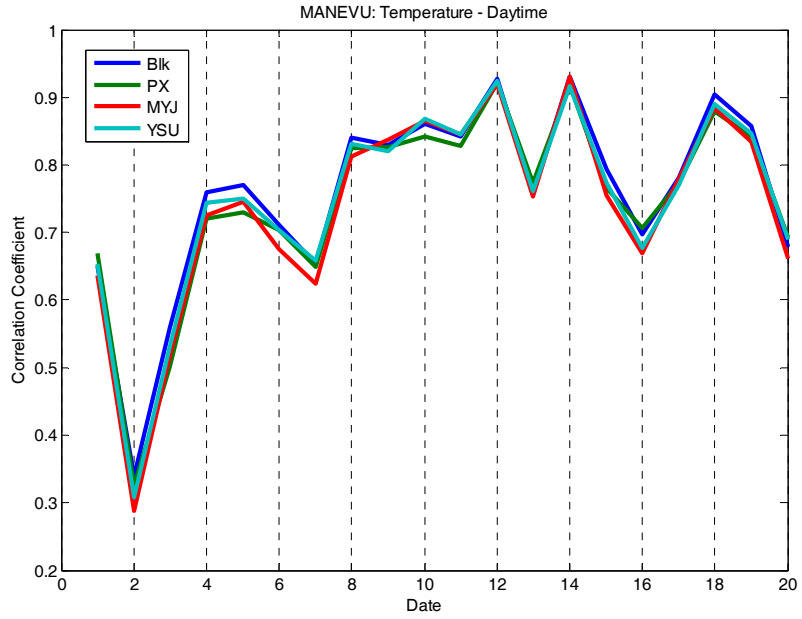

Looking at daytime temperatures in the summer, the BLK performs the best and the MYJ the worst in the correlation time series. The differences are up to 5%, larger than for the daily results.

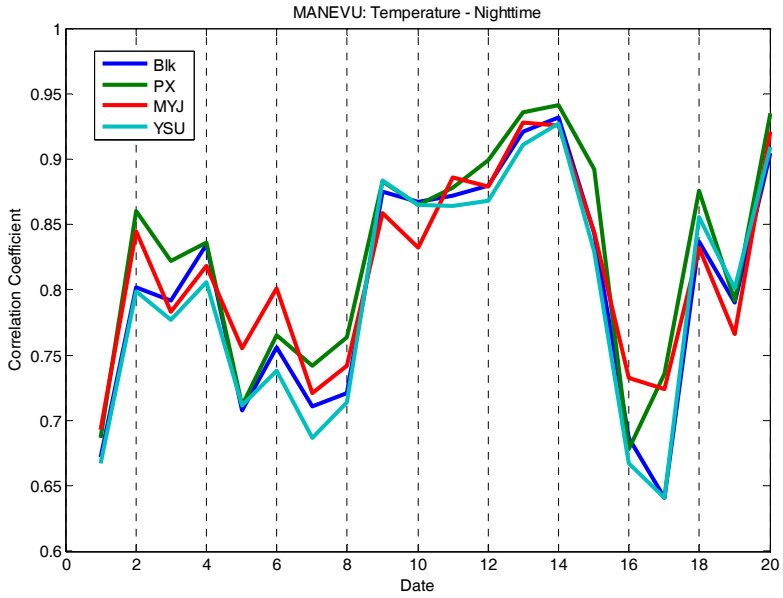

The largest spread of correlation coefficients for summer temperature is for the nighttime, with differences up to 10%. ACM2 fares the best under this category. On days that BLK and YSU have significant problems but MYJ improves, and vice versa.

The bias data for more urban TDL sites show that all PBL schemes performed similarly by overestimating summer daytime maximum temperature and underestimating nighttime minimum temperature (not shown). For the more rural CASNet temperature, ACM2 overestimated nighttime minimum temperature. The other three schemes overestimated

daytime maximum temperature and underestimated nighttime minimum temperature (not shown).

A summary RMSE and CORR statistics in the OTC region for summer temperature is in the table below. RMSE units are K (°C).

	RMSE			**CORR**		
PBL	*24-Hours*	*Day*	*Night*	*24-Hours*	*Day*	*Night*
MYJ	2.23	2.36	2.25	0.914	0.837	0.871
YSU	2.34	2.33	2.44	0.910	0.838	0.862
BLK	2.49	2.33	2.66	0.912	0.844	0.868
ACM2(PX)	2.38	2.43	2.41	0.901	0.827	0.835

The YSU results are similar to those in *Gilliam and Pleim* (2010) that found a RMSE of YSU at 2.31 K for summer temperatures. The same study had a lower RMSE of 1.94 for ACM2 (PX)—the difference is likely due to the 2-week soil moisture spin-up used in that study for ACM2. In *de Meij et al.* (2009), the YSU 2 m temperature RMSE was 2.0–4.4 K for June. *Akylas et al*. (2006) compared BLK, MRF, and MYJ PBL schemes in MM5 for the warm season and found that the BLK provided consistently good behavior for temperature forecasts. These results are also consistent with *Zhang & Zheng* (2004), which found that PBL schemes are able to recreate the diurnal cycles of temperature, however different schemes vary in temperature magnitude.

The plots for winter 2 m temperature are shown below for daily, daytime, and nighttime.

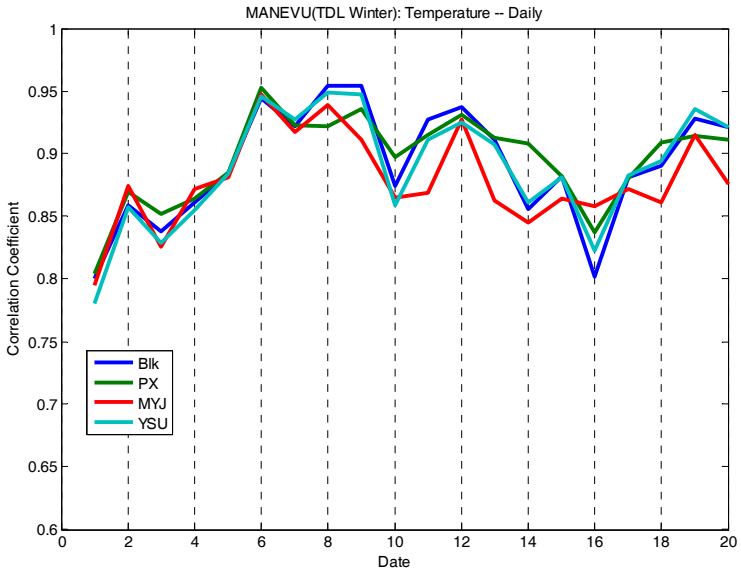

In the winter, there is more variability in daily temperature for different PBL schemes than for summer. Both ACM2(PX) and BLK do well for this variable while MYJ has some significant performance problems.

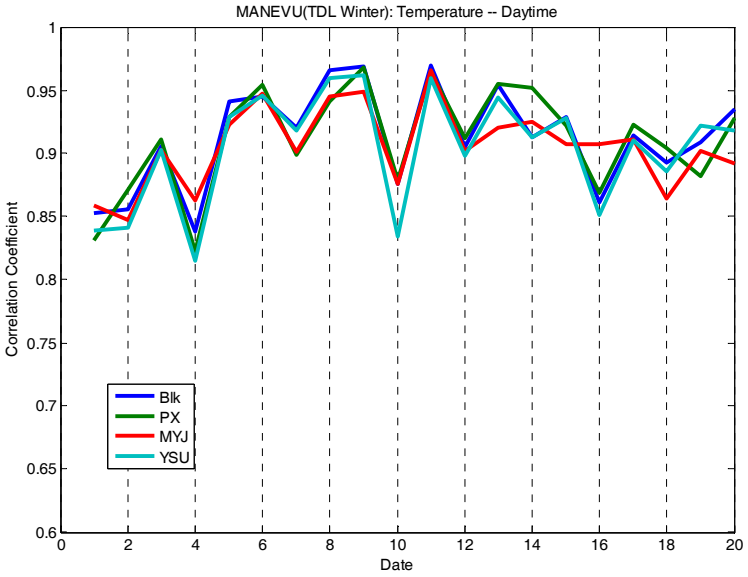

For daytime temperature, the winter statistics show that ACM2(PX) does well with BLK a close second but some big dips in correlation occur for MYJ and YSU.

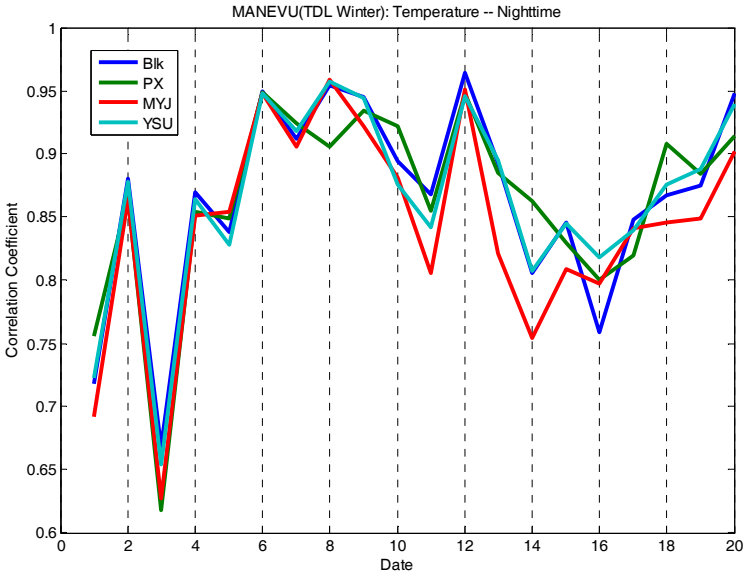

Looking at nighttime temperature in the winter, ACM2(PX) does the best in terms of correlation and MYJ does the worst.

The RMSE results confirm the correlation statistics. BLK and ACM2(PX) have lower error but tend to overestimate winter temperature and YSU and MYJ have higher error and tend to underestimate winter temperature. A summary RMSE and CORR statistics in the OTC region for winter temperature is in the table below. RMSE units are K (°C).

PBL	RMSE	CORR

	24-Hours	*Day*	*Night*	*24-Hours*	*Day*	*Night*
MYJ	2.83	2.09	3.19	0.894	0.929	0.872
YSU	2.46	2.07	2.62	0.915	0.933	0.903
BLK	2.45	1.91	2.64	0.918	0.942	0.907
ACM2(PX)	2.39	2.01	2.58	0.919	0.940	0.903

The domain-averaged RMSE for winter temperature are similar to those reported by *Gilliam and Pleim* (2010) for ACM2(PX): 2.48 K. Their RMSE results for YSU were lower: 2.33 K but they reported a large diurnal bias: warm bias at night and cold bias in daytime. Regionally, YSU had a lower temperature RMSE compared to the ACM2(PX) across most of the Eastern U.S. but higher for the Appalachian Mountains. In *de Meij et al.* (2009), YSU 2 m temperature RMSE was closer to the values in the table: 2.0–4.4 K for January. For the cold season, *Titov et al.* (2007) found similar correlation coefficients for 2 m temperature: BLK: 0.87 and ACM2(PX): 0.82.

7.2.2 Water Vapor Mixing Ratio

Observations of 2 m water vapor mixing ratio were compared with the results of each PBL scheme for both summer and winter periods. The New York modeling center created correlation plots for summer 2 m water vapor mixing ratio in the MANE-VU region divided into daily, daytime and nighttime.

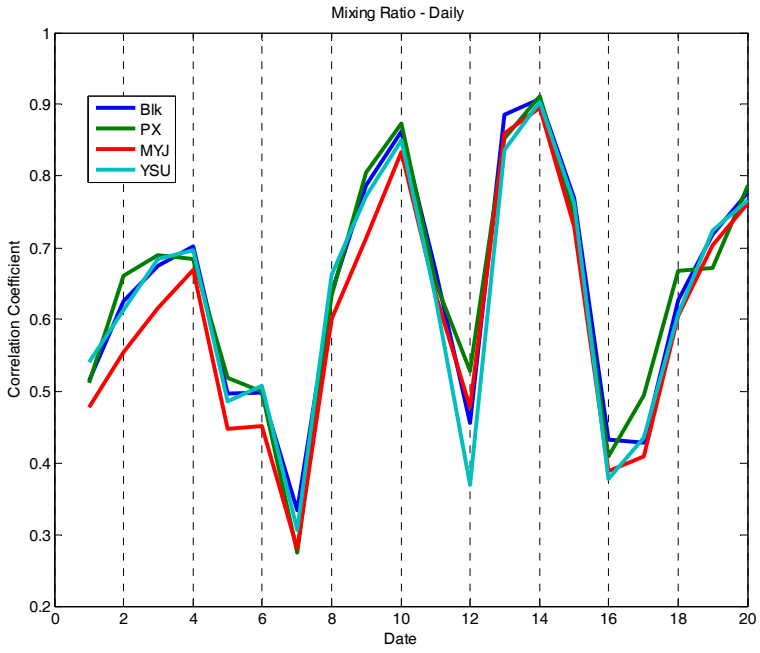

The results for water vapor mixing ratio were disappointing for all of the PBL schemes, with correlations ranging from 25–90%. For the daily moisture in summer, BLK and ACM2(PX) had similar correlation performance but YSU and MYJ had slightly larger drops in correlation for "bad days."

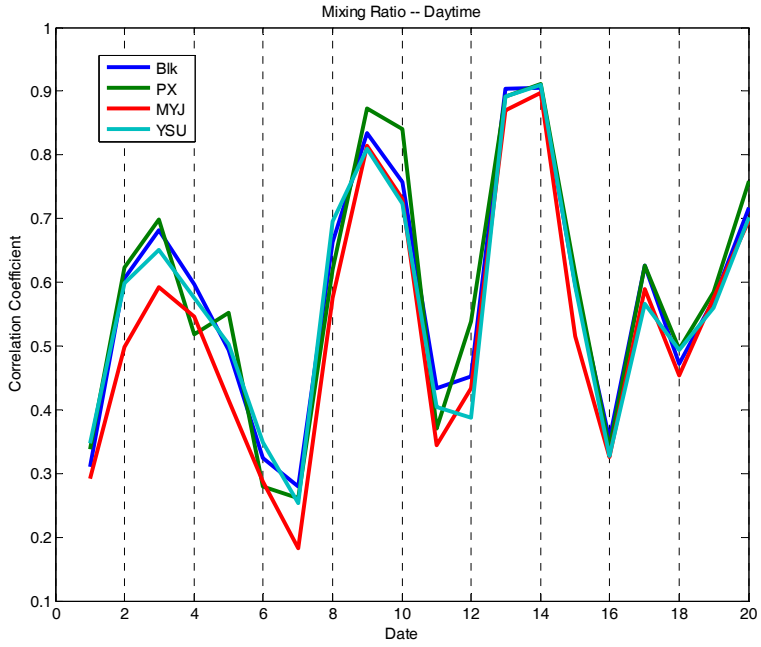

Looking at summer daytime temperatures, correlation performance is similarly poor but ACM2(PX) and BLK tend to do slightly better. MYJ had serious deficiencies for water vapor mixing ratio, dropping as low as 20% in correlation.

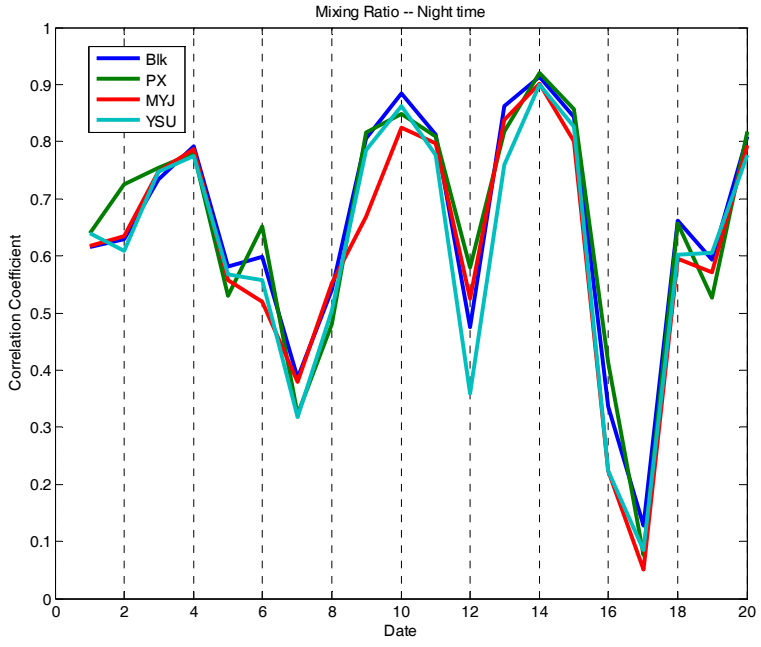

The PBL schemes have comparable correlations at night, with BLK the best and ACM2(PX) a close second. However, overall performance is still poor with one day under 10% correlations for all parameterizations.

The bias data for summer water vapor mixing ratio indicates that ACM2(PX) is the closest to the observations. BLK tends to overestimate humidity in the second part of the summer simulation. YSU always underestimates humidity (not shown). A summary RMSE and CORR statistics in the OTC region for winter water vapor mixing ratio is in the table below. RMSE units are g kg^{-1}.

PBL	**RMSE**			**CORR**		
	24-Hours	*Day*	*Night*	*24-Hours*	*Day*	*Night*
MYJ	2.00	2.06	1.95	0.787	0.783	0.807
YSU	2.15	2.13	2.27	0.804	0.805	0.806
BLK	1.94	1.94	1.98	0.815	0.817	0.830
ACM2(PX)	1.90	1.90	1.84	0.804	0.823	0.798

Gilliam and Pleim (2010) similarly found that YSU had the highest RMSE (1.92 g kg^{-1}) and ACM2(PX) had the lowest (1.86 g kg-1). In *de Meij et al.* (2009), YSU 2 m relative humidity RMSE was 12–17% for June.

The plots for winter water vapor mixing ratio are shown below for daily, daytime, and nighttime.

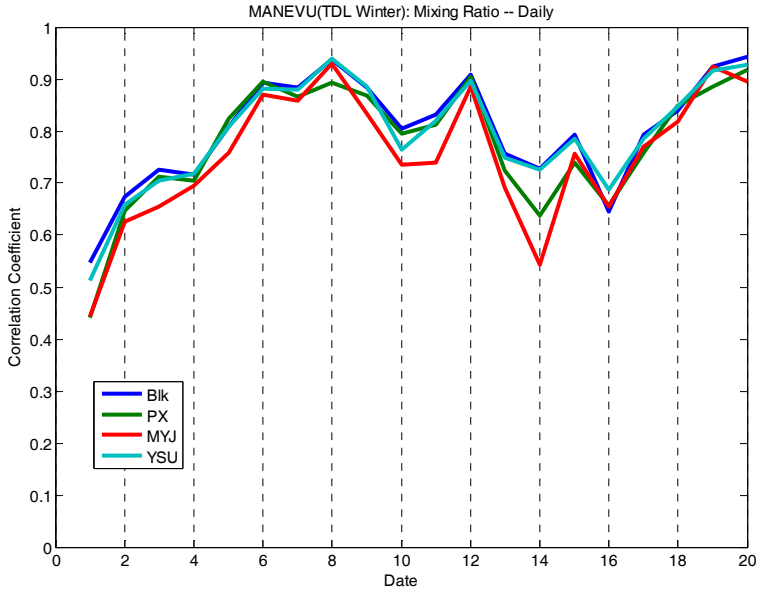

The winter moisture correlation results were far superior to the summer statistics. BLK has the best performance with YSU a close second. MYJ continues to perform poorly compared to the other schemes.

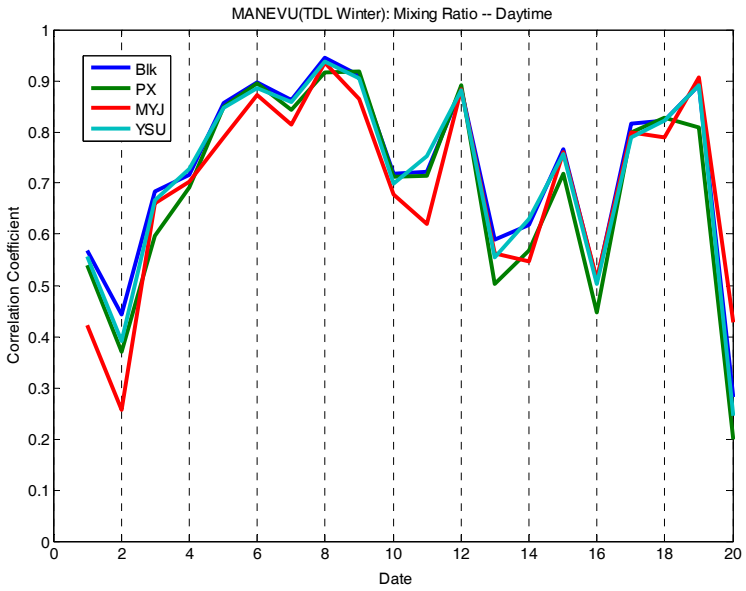

Focusing on daytime water vapor in the winter, MYJ continues to bring up the rear. BLK again has the best performance but ACM2(PX) and YSU are comparable.

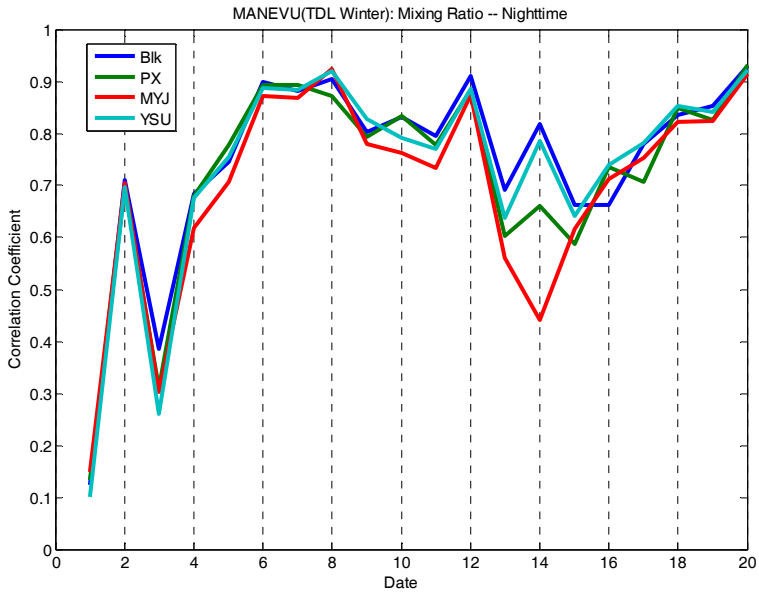

Despite poor performance by all four PBL schemes for nighttime moisture at the beginning of the winter period, probably due to inadequate spin-up, the schemes do quite well for the rest of the winter test period. BLK has the best correlation performance for winter water vapor mixing ratio, with YSU a close second. MYJ continues to experience significant problems with humidity measures.

In terms of RMSE, ACM2(PX) does slightly worse than MYJ and YSU slightly better than BLK, with a clear division between these two sets of schemes. A summary RMSE

and CORR statistics in the OTC region for summer water vapor mixing ratio is in the table below. RMSE units are g/kg.

PBL	RMSE			CORR		
	24-Hours	*Day*	*Night*	*24-Hours*	*Day*	*Night*
MYJ	0.76	0.80	0.73	0.883	0.887	0.878
YSU	0.65	0.68	0.63	0.913	0.911	0.912
BLK	0.67	0.69	0.65	0.919	0.917	0.919
ACM2(PX)	0.78	0.84	0.73	0.890	0.885	0.895

In contrast to the results reported above, *Gilliam and Pleim* (2010) found that YSU had the lowest RMSE (0.78 g kg-1) and ACM2(PX) had the highest (0.92 g kg-1). Again, the 10-day soil moisture spin-up for ACM2(PX) probably improved its performance. For the cold season, *Titov et al.* (2007) found lower correlations for relative humidity: BLK: 0.69 and PXP: 0.62. In *de Meij et al.* (2009), YSU RMSE for 2 m relative humidity was 10–18% for January.

7.2.3 Wind

Observations of 10 m wind direction and temperature were compared with the results of each PBL scheme for both summer and winter periods. Wind direction was examined early on but did not distinguish among the different parameterizations. This is not surprising since *Borge et al.* (2008), *Akylas et al.* (2006), and other studies have determined that wind direction is not clearly influenced by different PBL (or microphysics) schemes. As a result, OTC sensitivity tests focused primarily on wind speed.

Early PBL scheme tests identified serious problems in the wind speed simulations. The wind speed results for the YSU and MYJ showed a serious overestimation and delayed diurnal cycle for winds. This issue can be seen most clearly in the results for CASTNet (mostly rural) sites. The summer results are below:

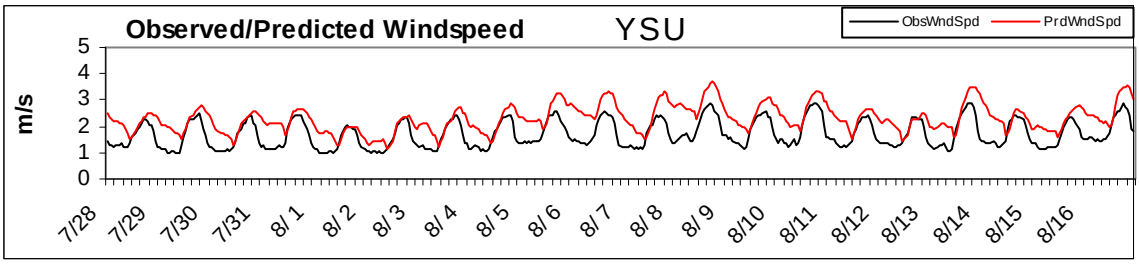

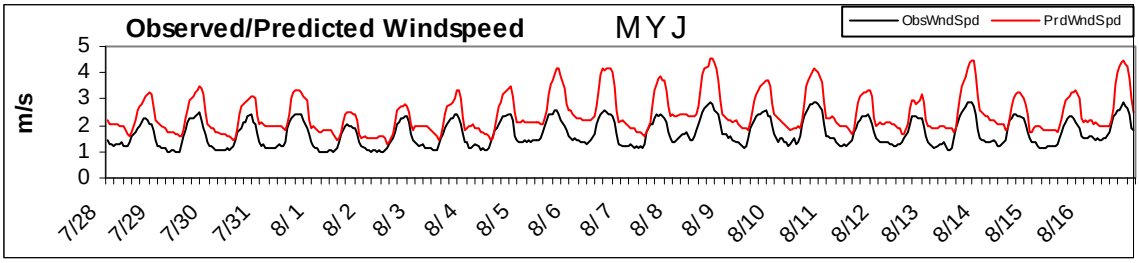

The wind speed problem was also apparent during the winter period for YSU and MYJ:

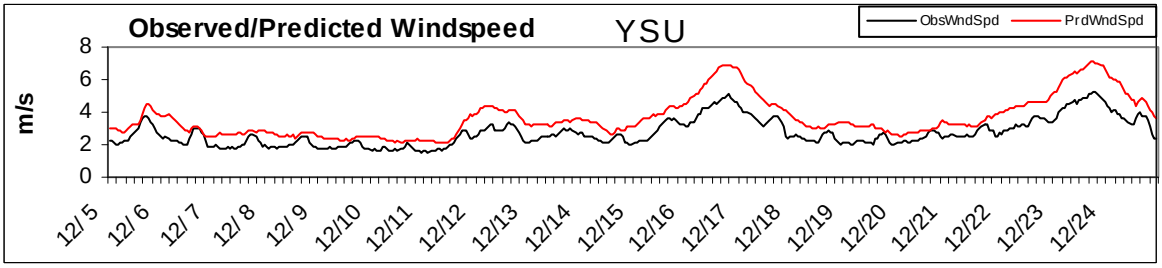

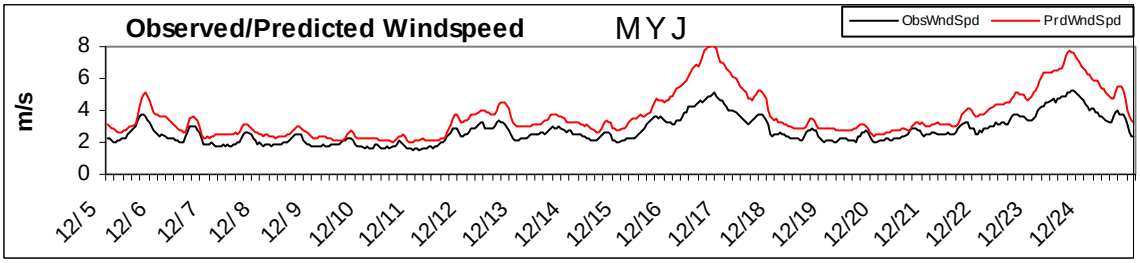

As mentioned above, the response to this issue was to add BLK to the list of PBL schemes to be tested because it had shown good performance in diurnal wind speeds when used in MM5.

One of the questions that arose in the WRF Work Group was the use of calm winds for evaluation. Comparisons of TDL wind speed with and without calm measurements were developed by the New York modeling center and are shown below. It is clear that the case without including TDL zero wind speed data, the ACM2 scheme has serious underpredicting the daytime peak wind speed (blue line in the third panel of the following plots).

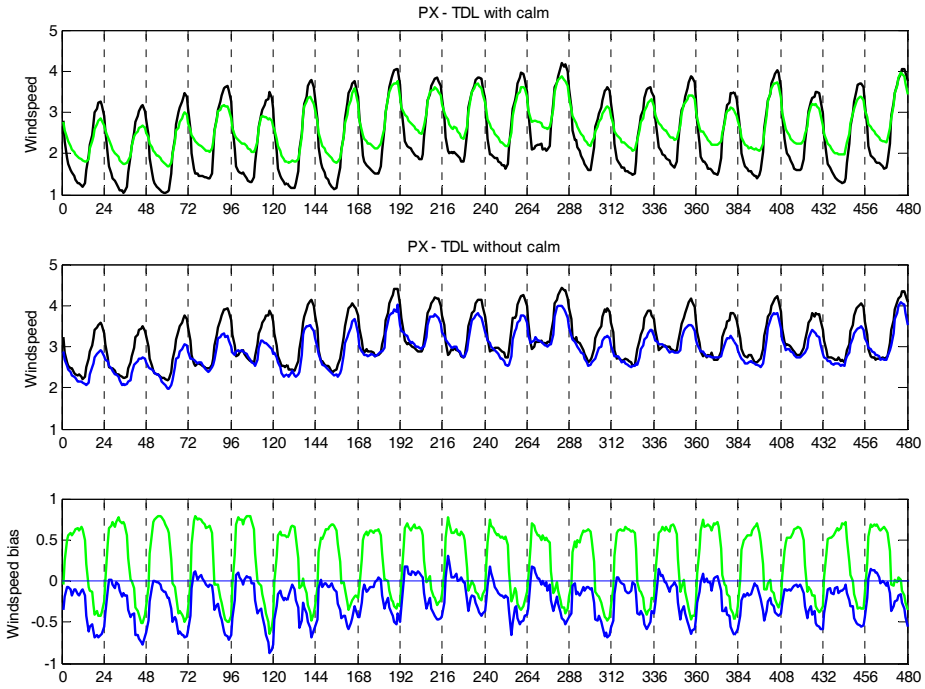

These results show that removing calm wind data would reduce the nighttime low wind speed bias but it also increase the bias slightly in daytime wind speed. Removing calm wind data also increased average temperature and humidity. OTC decided to include calm wind observations for the WRF sensitivity tests.

Once these issues were addressed, the same evaluation process used for temperature and water vapor mixing ratio was applied to wind speed. The New York modeling center created correlation plots for summer 10 m wind speed in the MANE-VU region divided into daily, daytime and nighttime.

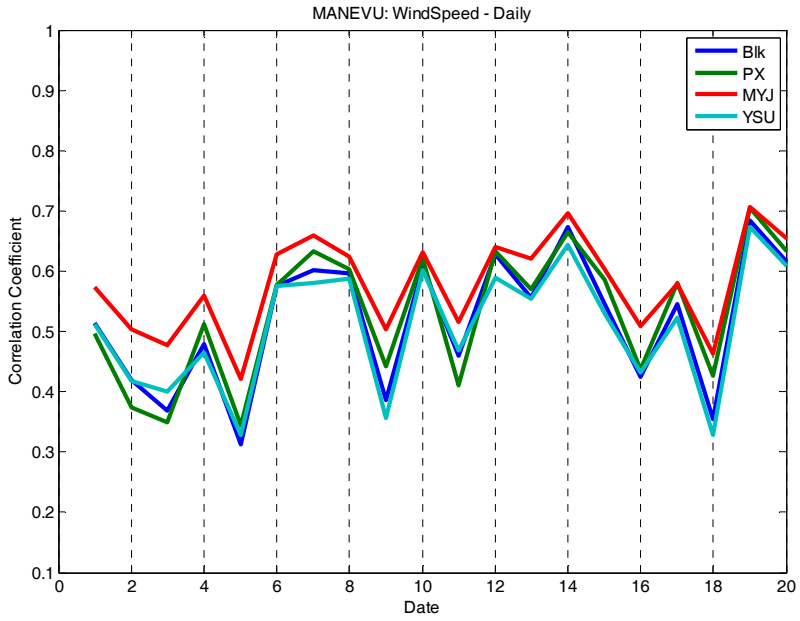

Looking at daily correlation, MYJ turned out to do quite well for summer wind speed. ACM2(PX), BLK, and YSU all performed comparably to each other.

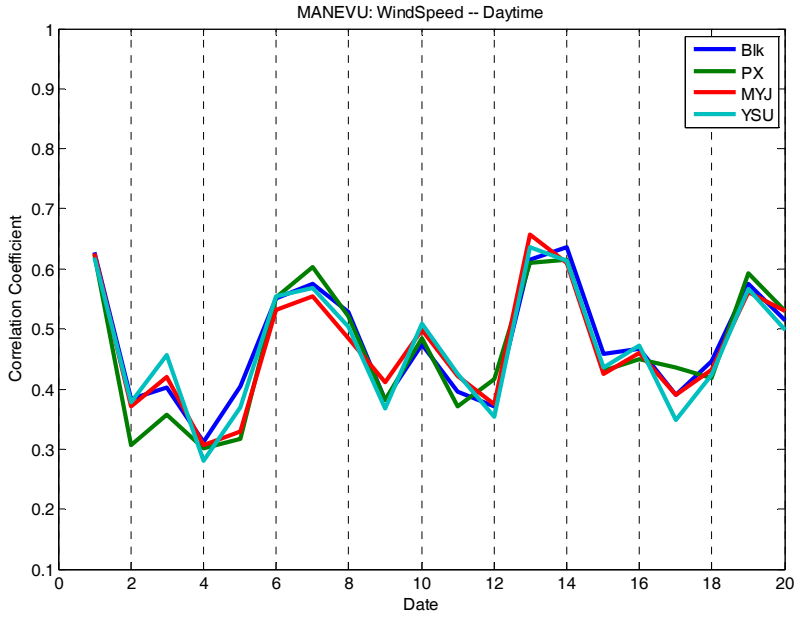

The summer daytime wind speed showed a different ranking, with ACM2(PX) and BLK taking the lead. However, there was not much difference among the four schemes.

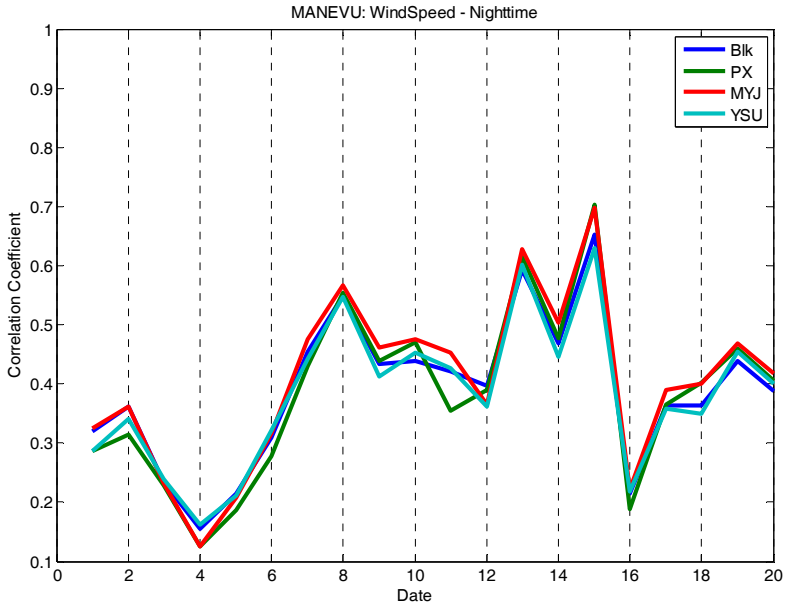

It was nighttime wind speeds for which MYJ generally outperformed the other schemes, but overall performance at night was uniformly poor.

However, the RMSE scores showed that ACM2(PX) had the lowest errors for daily and daytime wind speed in the summer but the differences among the PBL schemes were small: up to 0.11 m s^{-1} (about 6% gross error). A summary RMSE and CORR statistics in the OTC region for summer wind speed is in the table below. RMSE units are m s^{-1}.

PBL	**RMSE**			**CORR**		
	24-Hours	*Day*	*Night*	*24-Hours*	*Day*	*Night*
MYJ	1.70	1.77	1.69	0.630	0.595	0.486
YSU	1.74	1.72	1.80	0.575	0.591	0.478
BLK	1.72	1.79	1.72	0.585	0.597	0.479
ACM2(PX)	1.70	1.69	1.72	0.599	0.595	0.486

Gilliam and Pleim (2010) had similar results for summer wind speed RMSE: ACM2(PX) (1.47 m s^{-1}) did better than YSU (1.60 m s-1). In *de Meij et al.* (2009), YSU wind speed RMSE was higher: 2.7 m s^{-1} for June. *Akylas et al.* (2006) compared BLK, MYJ, and a third scheme (MRF) in MM5 for the warm season and found that the BLK provided consistently good behavior for wind forecasts.

The plots for winter water vapor mixing ratio are shown below for daily, daytime, and nighttime.

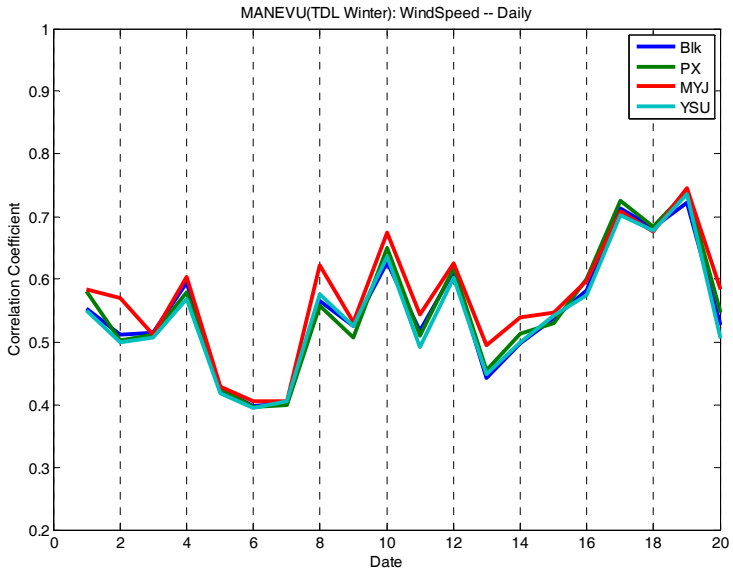

Observations of daily wind speeds were more strongly correlated to MYJ in the winter test period, although differences among the four schemes were minor.

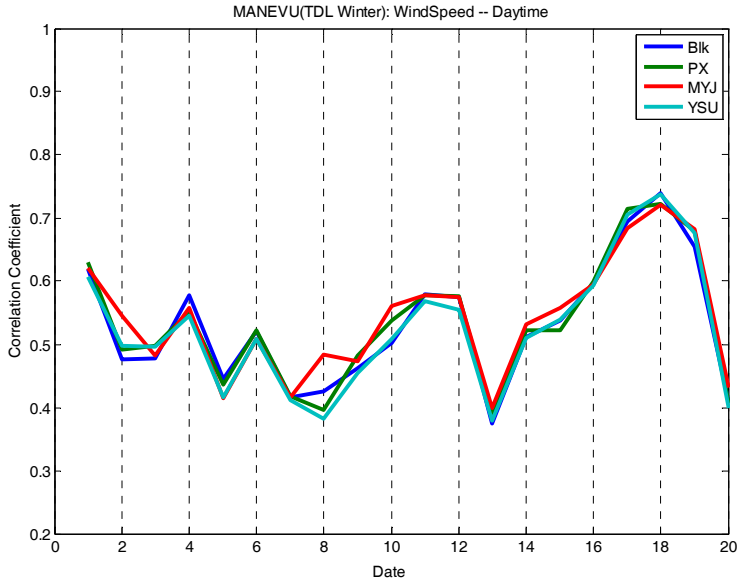

During the daytime, the results are almost indistinguishable among the four PBL schemes.

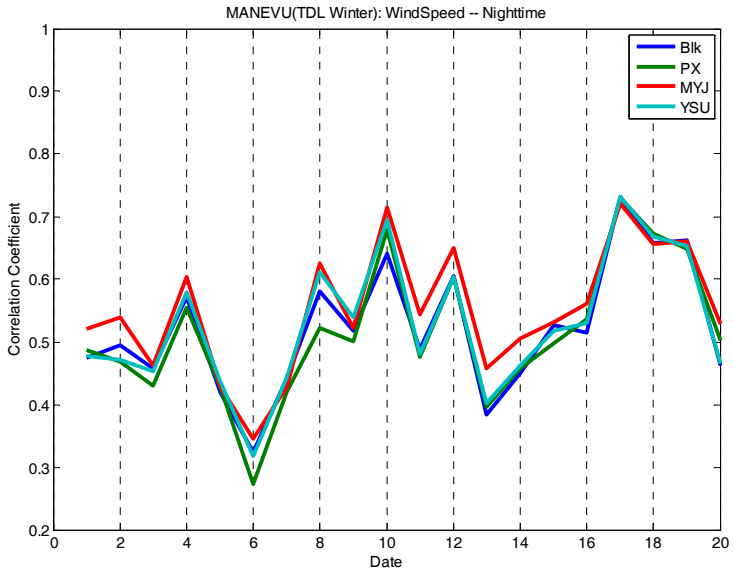

As in summer, MYJ has stronger correlations with nighttime wind speed but performance of all four PBL schemes is disappointing.

Looking at bias, winter TDL wind speed showed more stable in ACM2(PX) results, YSU suffered a high bias, while BLK and MYJ results varied (not shown). For the winter CASTNET wind speed, all schemes overestimated wind speed but BLK was better than the other three (not shown). A summary RMSE and CORR statistics in the OTC region for winter wind speed is in the table below. RMSE units are m s^{-1}.

PBL	**RMSE**			**CORR**		
	24-Hours	*Day*	*Night*	*24-Hours*	*Day*	*Night*
MYJ	2.18	2.15	2.20	0.692	0.696	0.697
YSU	2.22	2.17	2.23	0.692	0.690	0.707
BLK	2.18	2.15	2.20	0.692	0.696	0.697
ACM2(PX)	2.17	2.11	2.21	0.695	0.705	0.694

Gilliam and Pleim (2010) found that for winter wind speed, the RMSE for ACM2(PX) (1.64 m s-1) did better than YSU (1.78 m s-1). In *de Meij et al*. (2009), YSU wind speed RMSE was 2.7 m s-1 for January. For the cold season, *Titov et al.* (2007) found slightly lower correlations for wind speed: BLK: 0.62 and ACM2(PX): 0.63.

7.2.4 Precipitation

Accuracy in the magnitude and spatial distribution of precipitation is important for air quality simulation. It affects wet deposition of soluble chemical species like NO_x, which is important for both ozone and $PM_{2.5}$. Predicting convective precipitation in summer is a still challenging for mesoscale models. For the PBL scheme sensitivity tests, the New York modeling center took 24-hour accumulated precipitation in mm ending for a four days (August 2–6) and compared it to NCEP Stage 4 Gridded Data derived from a combination of radar and rain gauges

(http://www.emc.ncep.noaa.gov/mmb/ylin/pcpanl/stage4). The dataset did not include rain over the ocean although all simulations did.

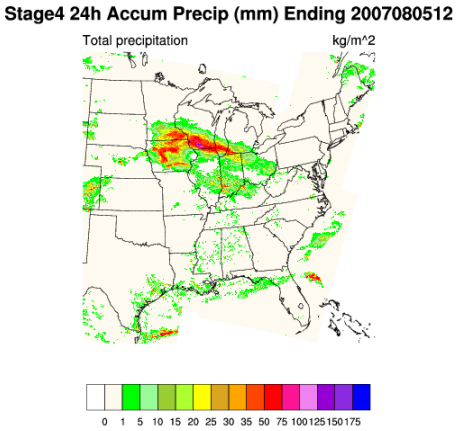

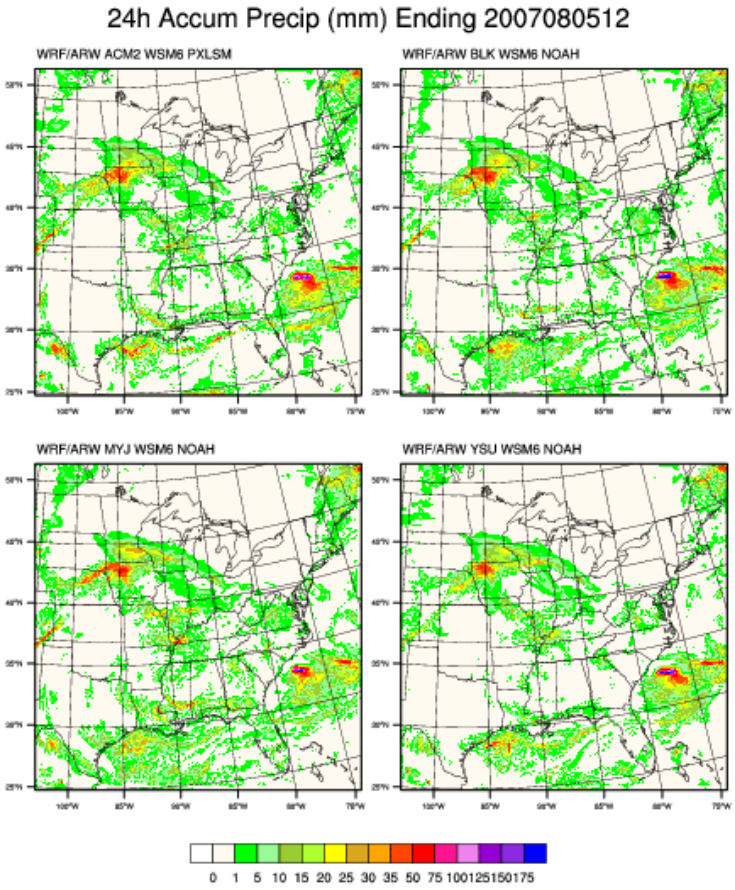

For all the days, the spatial configuration and magnitude of precipitation was similar for all four PBL schemes. The biggest differences from the observations could be seen on August 5 (shown above). All the models overestimated precipitation in the Northeast, with ACM2(PX) having the largest magnitude error.

7.2.5 Cloud Cover

CMAQ ozone concentrations are highly sensitive to cloud cover from mesoscale meteorology models [*Lin et al*. 2009]. *Appel et al.* (2009) also found that the differences in their CMAQ modeling by using WRF and MM5 meteorological data were caused in part by differences in predicted cloud cover.

WRF outputs were processed through MCIP to get the model cloud fraction data. The observed gridded cloud fractions were derived based on satellite-measured surface radiation and is available at the UMD website (http://www.atmos.umd.edu/~srb/gcip/gsipsrb). The following plots show an example of comparison for cloud fraction at 17:00Z August 5.

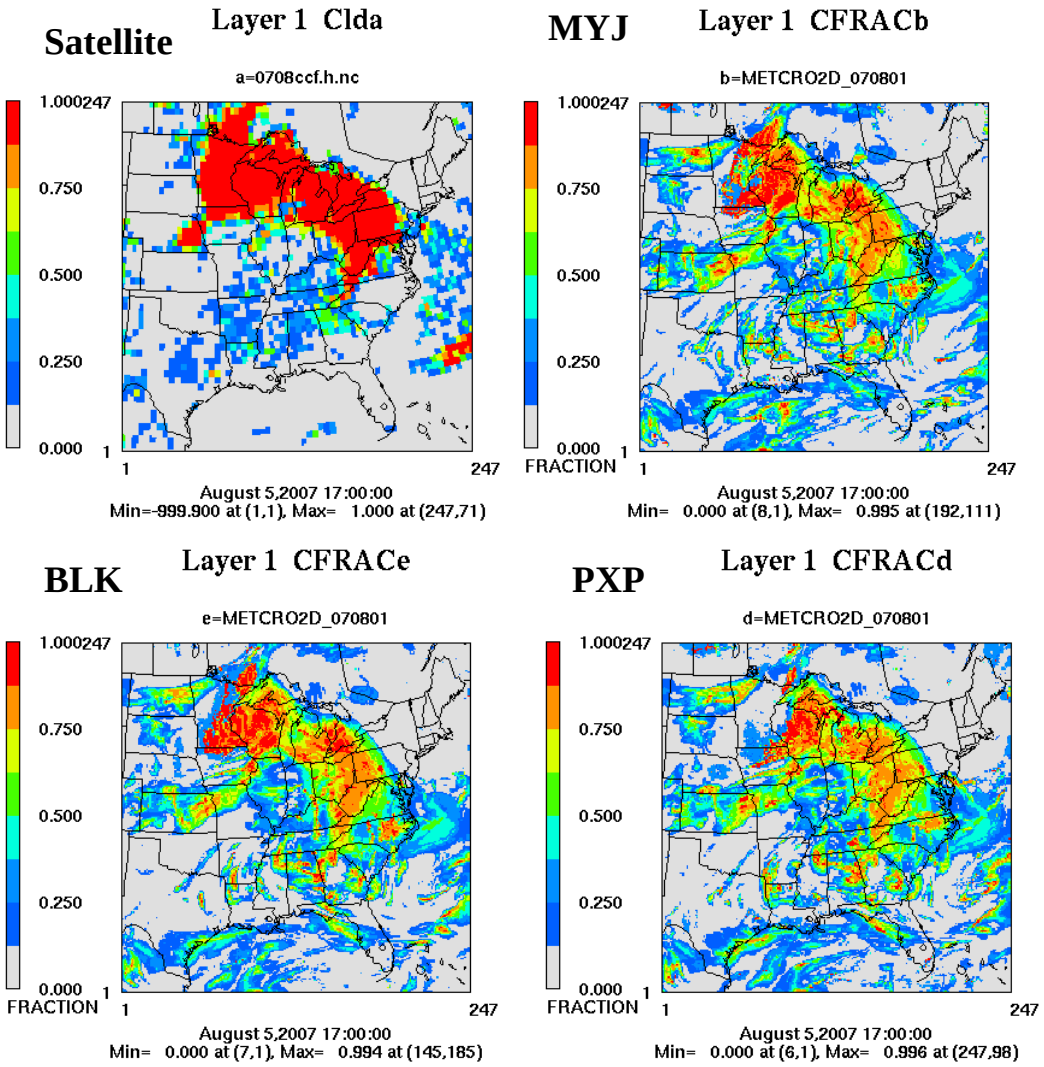

The three PBL schemes tested (MYJ, BLK, and ACM2(PX)) produced similar cloud fraction pattern with each other and the model results were comparable with satellite cloud coverage pattern.

7.2.6 Vertical Profiles

Winds in the free troposphere play an important role in regional transport of ozone, $PM_{2.5}$, and their precursors so the impact of the different PBL schemes on the vertical wind distribution was evaluated. The New York modeling center compared wind profiler data with WRF simulations for all four PBL schemes: YSU, MYJ, BLK, and ACM2(PX). Wind profiler observation data were available at the Meteorological Assimilation Data Ingest System (MADIS) network at http:/ madis.noaa.org. The wind profilers were located in Beltsville, MD (BLTMD), New Brunswick, NJ (RUTNJ), and Stow, MA (STWMA). Comparisons were made for four different times during the 24-hour period: 00z, 06z, 12z, and 18z at each location. They considered YSU along with MYJ, BLK, and ACM2(PX). Here are samples from August 2 for BLTMD:

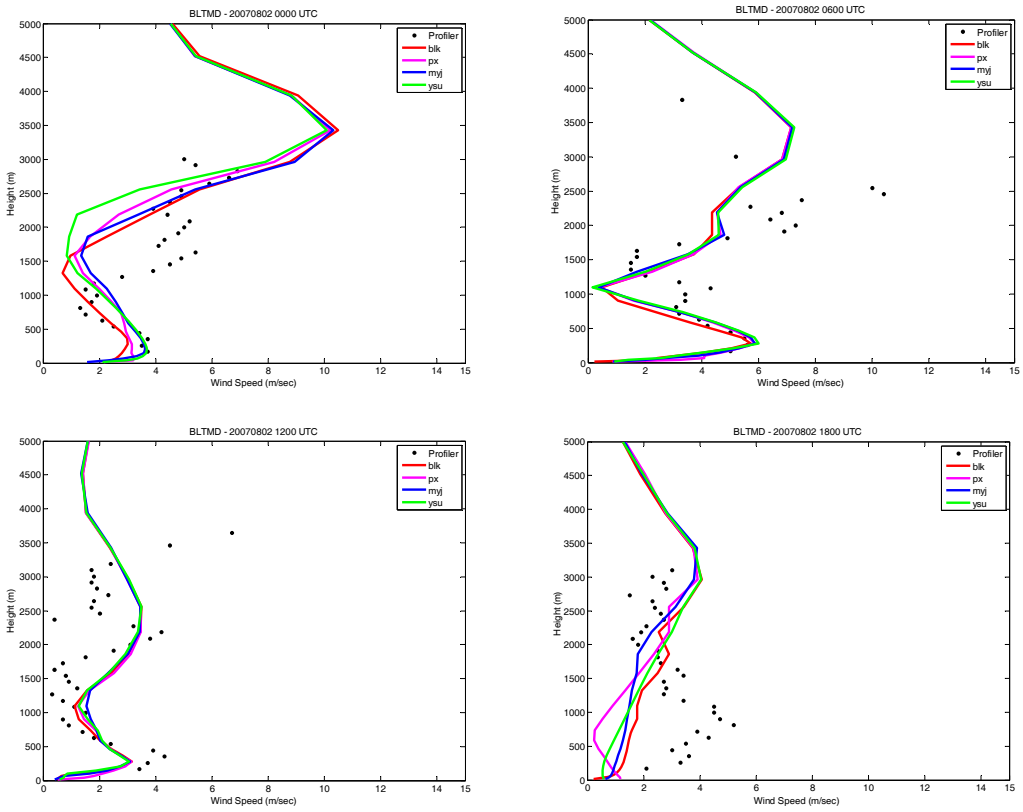

In BLTMD, the biggest differences in the profiles occurred at 8:00 pm EDT (00z) and 2:00 pm EDT (18z). While all performed poorly during the afternoon, BLK captured the evening profile better than the other PBL schemes.

The results in RUTNJ are shown below:

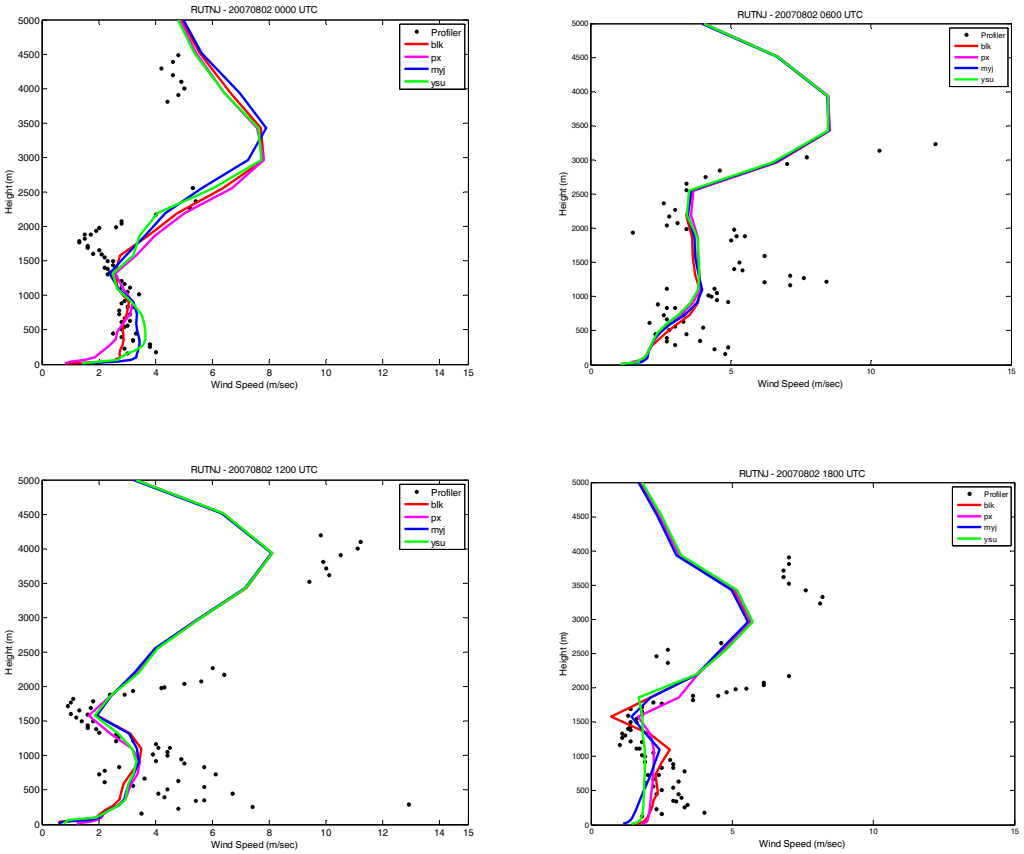

For RUTNJ, the vertical profiles are very close for 2:00 am EDT (06z) and 8:00 am EDT (12z), but all four have magnitude problems between 1.5 and 2.0 km at 8:00 pm EDT (00Z). Both BLK and MYJ capture the wind shear pattern below 2 km at 2:00 pm EDT (18z). Results for STWMA are similar (not shown).

One of the reasons for changing from MM5 to WRF is reports that WRF is better able to simulate mesoscale wind patterns like found the nocturnal low level jets (NLLJ) [*Gilliam et al.* 2009]. A NLLJ between the Appalachian Mountains and the East Coast moving from North Carolina to Massachusetts occurs periodically and transports ozone, PM2.5, and precursors to the Northeast. To determine the impact of PBL schemes on simulations of this phenomenon, the August 2–3, 2007 event was simulated and compared to wind profiler observations for BLTMD, ROTNJ, and STWMA. Three PBL schemes were tested: MYJ, BLK, and ACM2(PX). The results for August 3 in Beltsville, MD are shown below:

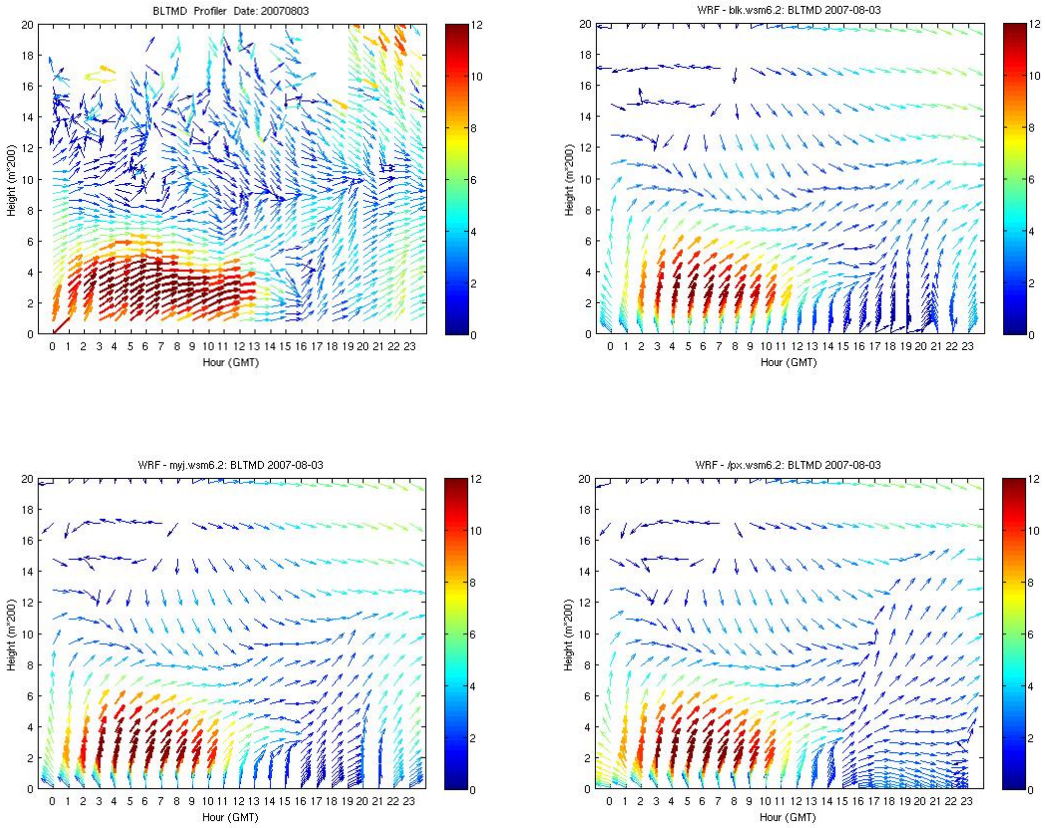

The NLLJ shows up clearly at the Baltimore wind profilers with a prolonged period of high winds overnight. The three PBL schemes are almost identical in their results. The simulations capture the magnitude of the jet and its vertical dimensions but underestimate the NLLJ duration.

For August 3 at Rutgers, New Jersey:

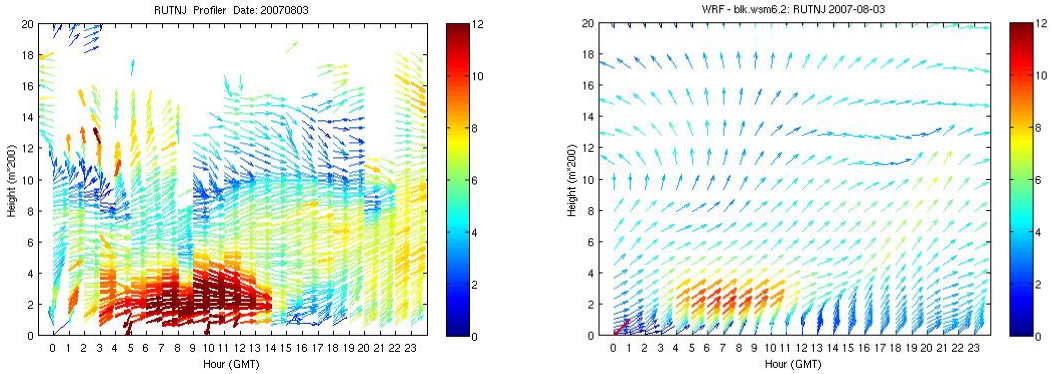

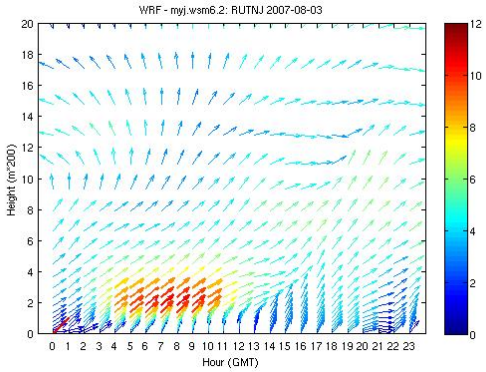

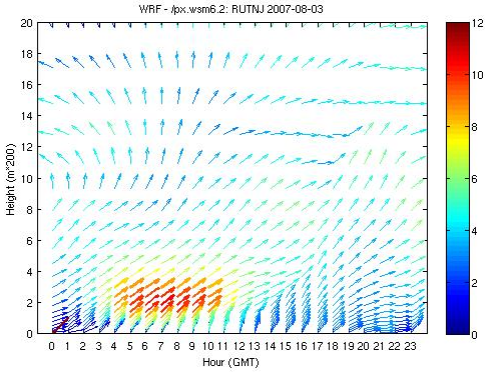

Again, the three PBL schemes show very similar results. The NLLJ feature appears in WRF but its duration, vertical dimensions, and magnitude are all underestimated.

The results for Stow, MA:

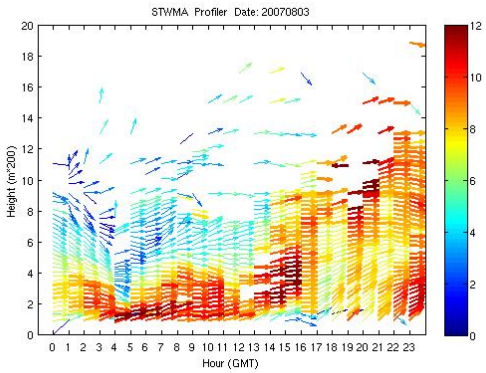

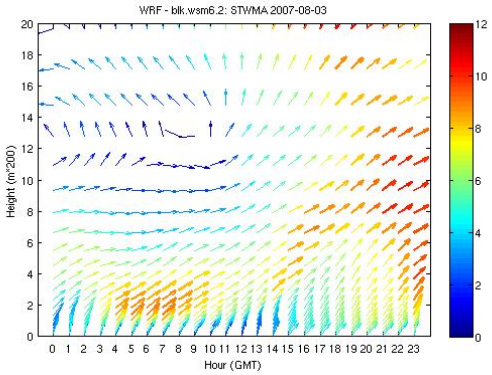

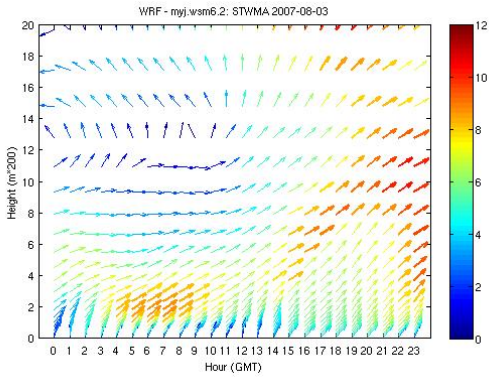

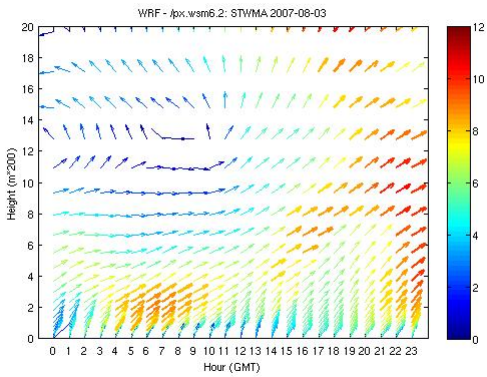

All three schemes captured the NLLJ feature reasonably well (along with the pattern of winds the following day). The underestimation of the NLLJ its duration, vertical dimensions, and magnitude appears to increase as more northerly locations.

Another upper air evaluation was to compare with Howard University ozonesonde data at Beltsville, MD to the simulations of vertical profiles of wind speed and mixing ratio and taken in the same area. Three PBL schemes were compared: MYJ, BLK, and ACM2(PX). A sample for 8/4/09 10:11z (6:11 am EDT) is shown below.

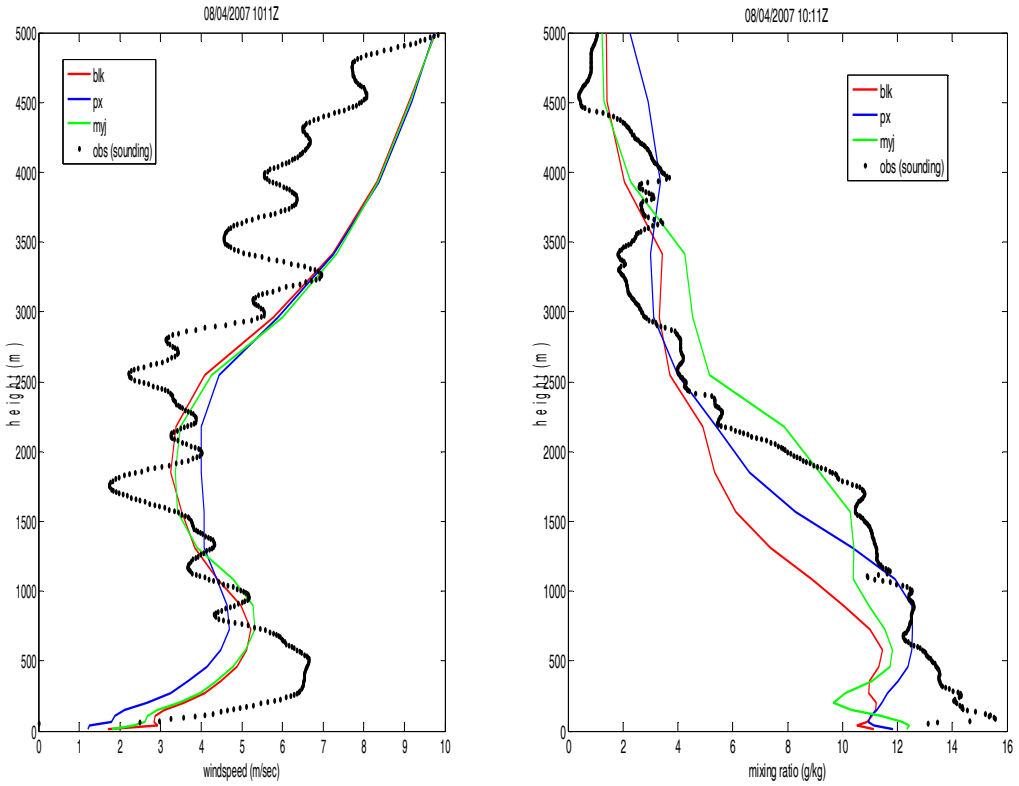

All three schemes reproduced a smooth version of the observation. ACM2(PX) did a particularly nice job of reproducing the moisture profiles.

7.3 Other Settings

While testing of all types of parameterizations occurred at the same time, this summary will note the highlights individually for each type of physics package.

7.3.1 Microphysics

Three microphysics parameterizations were tested as part of this effort [*Wang et al.* 2009]:

Name	Abbrev.	Description
WRF Single-Moment 5-Class	WSM5	A simple efficient scheme with diagnostic mixed-phase processes and super-cooled water
WRF Single-Moment 6-Class	WSM6	A scheme with ice, snow and graupel processes suitable for high-resolution simulations
Morrison Double-Moment	Morrison	Double-moment ice, snow, rain and graupel for cloud-resolving simulations. New in WRF v. 3.0.

The UMD and New York modeling centers evaluated the two microphysics schemes: WSM5 and WSM6. They ran these two schemes with each PBL scheme being evaluated (MYJ, YSU, BLK, and ACM2(PX)). They found WSM6 and WSM5 results to be similar in surface data comparisons. The Iowa modeling center ran tests with the Morrison microphysics scheme.

The choice of microphysics schemes is highly influential on precipitation [*Borge et al.* 2008] so assessment was made of this parameter in WRF simulation. The Iowa modeling center compared gridded precipitation observations for total accumulation for July 29 to August 16 compared to WRF precipitation output for ACM2(PX) with three different microphysics schemes (WSM5, WSM6, and Morrison). The simulation with Morrison is identified as PXEPA, to distinguish it from the other two microphysics schemes.

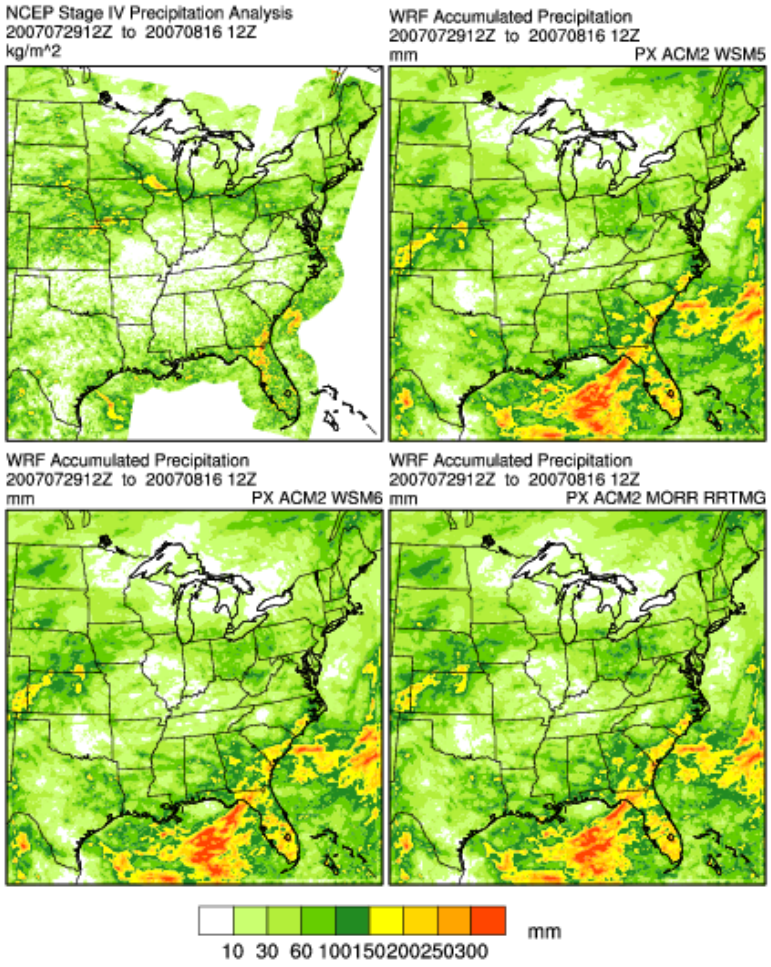

All three microphysics schemes overestimated accumulated precipitation, especially in the Southeast. The results in the Northeast were almost indistinguishable.

The Iowa modeling center also tested winter precipitation from December 6–24, 2007:

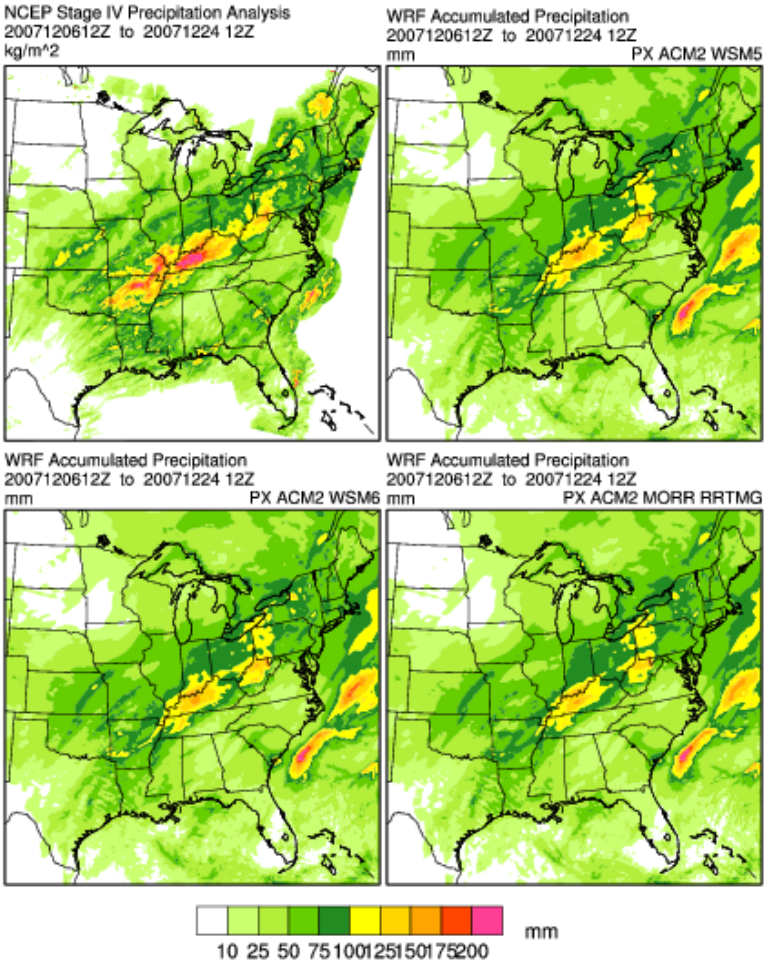

For winter, precipitation on land was underestimated by all three microphysics schemes but the spatial distribution was very good.

Iowa also chose four days to check 24-hour accumulations for a precipitation event in winter For December 16–17, 2007:

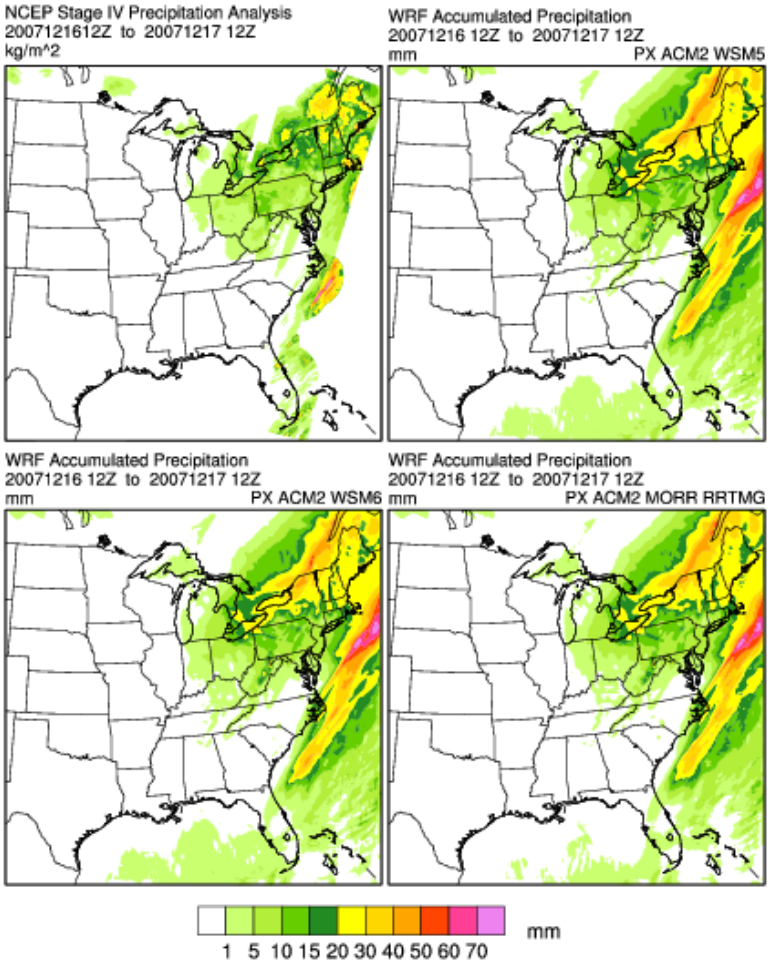

This case study also showed strong similarity among the simulations but all also overpredicted rain in the Northeast.

Overall, the microphysics schemes all showed similar performance. In terms of computer resources, WSM6 was the most efficient scheme and as such it was adapted for the WRF production run.

7.3.2 Land Surface

Three land surface models were tested in WRF [*Wang et al.* 2009]:

Name	Abbrev.	Description
Slab	SLAB	Simple 5-layer thermal diffusion schemes using soil temperature only for five layers.
Noah	NOAH	Unified NCEP/NCAR/AFWA scheme with soil temperature and moisture in four layers, fractional snow cover and frozen soil physics. New modifications were added in Version 3.1 to better represent processes over ice sheets

Name	Abbrev.	Description
Pleim & Xiu	PX LSM	and snow covered area Two-layer scheme with vegetation and sub-grid tiling. New in WRF v. 3.0

Tests run by the UMD compared the SLAB and NOAH land surface models and presented their results. Surface temperature and moisture improved with NOAH. They found that the SLAB resulted in large wind speed biases of up to 2-3 m s^{-1}. The runs with NOAH cut this bias in half (not shown).

The New York modeling center compared NOAH and PXLSM for runs with BLK and WSM6. Three variations of the PXLSM were used. One used the soil moisture program IPXWRF to initialize PXLSM. Another did a restart of PXLSM to determine if there was any periodic bias in PXLSM. Finally, PXLSM was used without these two options. The statistics from these tests are shown in the table (please note that these RMSE were calculated with a difference formula to highlight daily variations and are not comparable to other RMSE calculations in this report):

RMSE for:	Season	Land	Day	Night	24-hrs
Temperature (K)	Summer	NOAH	2.48	2.31	2.63
		PX LSM	2.28	2.40	2.24
		PXLSM (ipxwrf)	2.18	2.36	2.07
		PXLSM (restart)	2.17	2.34	2.07
	Winter	NOAH	2.39	1.86	2.54
		PXLSM	2.13	1.69	2.29
		PXLSM (ipxwrf)	2.15	1.67	2.34
		PXLSM (restart)	2.15	1.67	2.34
Mixing Ratio (g kg^{-1})	Summer	NOAH	1.91	1.91	1.93
		PXLSM	1.94	1.99	1.73
		PXLSM (ipxwrf)	1.97	1.98	1.81
		PXLSM (restart)	1.96	1.98	1.79
	Winter	NOAH	0.65	0.67	0.63
		PXLSM	0.76	0.82	0.71
		PXLSM (ipxwrf)	0.74	0.80	0.68
		PXLSM (restart)	0.73	0.80	0.68
Wind Speed (m s^{-1})	Summer	NOAH	1.71	1.78	1.70
		PXLSM	1.69	1.73	1.63
		PXLSM (ipxwrf)	1.66	1.72	1.59
		PXLSM (restart)	1.66	1.72	1.59
	Winter	NOAH	2.14	2.09	2.14
		PXLSM	2.12	2.05	2.13
		PXLSM (ipxwrf)	2.13	2.06	2.14
		PXLSM (restart)	2.13	2.06	2.14

The NOAH land surface model had the lowest error for water vapor mixing ratio, but PXLSM was superior in temperature and wind speed. Seasonal differences were minor. For the different PXLSM variations, IPXWRF did not significantly improve the results and restarts performed as well as cold start runs with no drift from observations. No cyclic error was detected.

7.2.3 Radiation

Two sets of longwave-shortwave radiation parameterizations were tested: RRTM with Dudhia and RRTMG:

Name	Abbrev.	Description
Rapid Radiative Transfer Model (Longwave)	RRTM	An accurate scheme using look-up tables for efficiency. Accounts for multiple bands, trace gases, and microphysics
Dudhia (Shortwave)	DUDH	Simple downward integration allowing efficiently for clouds and clear-sky absorption and scattering. When used in high-resolution simulations, sloping and shadowing effects may be considered
RRTM for GCM Applications (Longwave and Shortwave)	RRTMG	A reduced form of RRTM designed for climate models. Includes the Monte Carlo Independent Cloud Approximation method of random cloud overlap. New in WRF v. 3.1.

The Dudhia shortwave and RRTM longwave schemes have been used extensively for air quality modeling by New York and UMD, along with many other researchers. The Iowa modeling center utilized the new RRTMG radiation scheme in their run previously identified as PXEPA. The tests were for RRTMG were run only for the ACM2 (PX) PBL scheme (red line below) while all the other PBL schemes (BLK, MYJ, and YSU) were run with RRTM/DUDH. Only the summer season was tested because radiation schemes have the most impact on ozone levels.

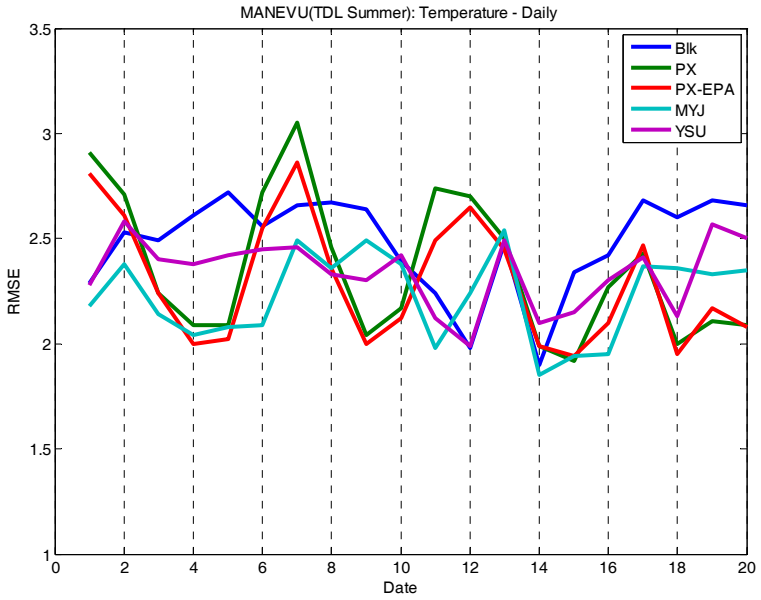

Not surprisingly, the biggest differences were for temperature. The RRTM/DUDH in general shows more consistent RMSE performance. There was a tendency for RRTMG to have significant increases in error for specific days.

Radiation also has an impact on evaporation so water vapor mixing ratio results were compared for the two sets of radiation schemes.

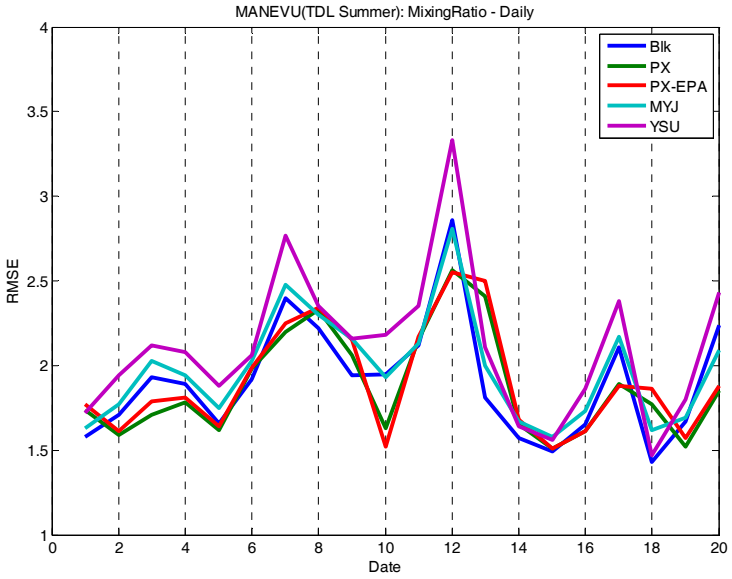

For mixing ratio, RRTMG performs consistently better than RRTM/DUDH.

Since pressure differences are affected by radiation through surface heating, the wind speed was also compared for different radiation schemes.

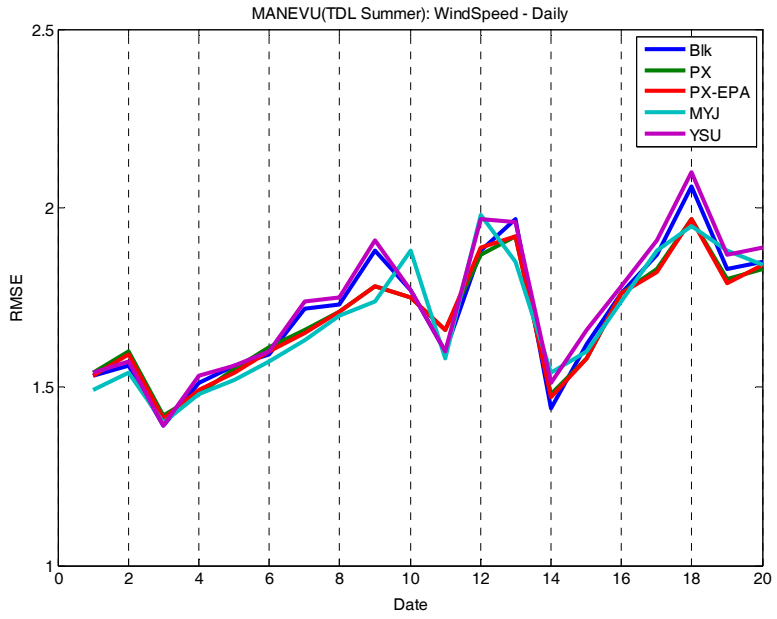

There was little difference between RRTM/DUDH and RRTMG for wind speed results. One concern raised by the tests was that the RRTMG scheme added a considerable amount of run-time for the simulations.

7.4 Final Selection of WRF Parameterizations

Selecting the *planetary boundary layer* scheme based on sensitivity tests discussed above was very difficult. It became obvious during testing that the nonlocal schemes, BLK and ACM2(PX) were better in general compared to the local schemes, YSU and MYJ. One of the concerns raised in the WRF Work Group was the fact that BLK had not been officially released for WRF. Rob Gilliam of EPA compared BLK to the ACM2(PX) results on the EPA platform for one short period of July 31 to August 2, 2006. One difference to the tests discussed above is that the ACM2(PX) was run with a more up-to-date and specialized land use data from National Land Cover Database (NCLD). The results for 2 m temperature, 2 m water vapor mixing ratio, and 10 m wind speed are displayed below.

2-m Temp

ACM2 – PX

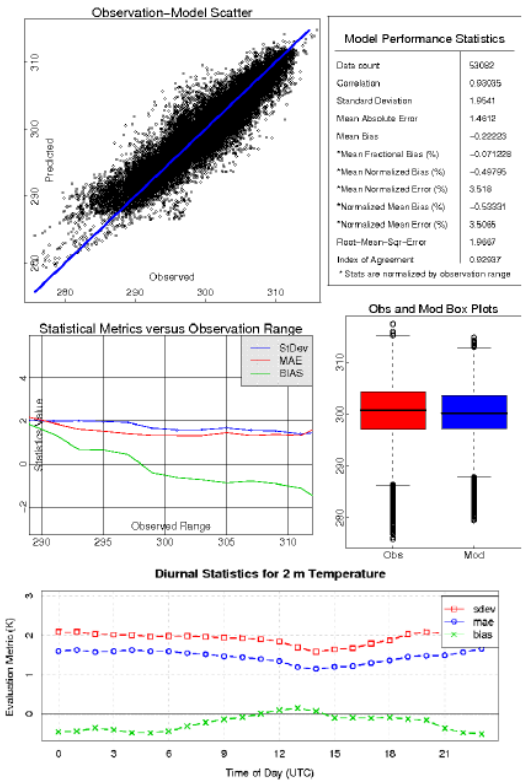

Blackadar – PX

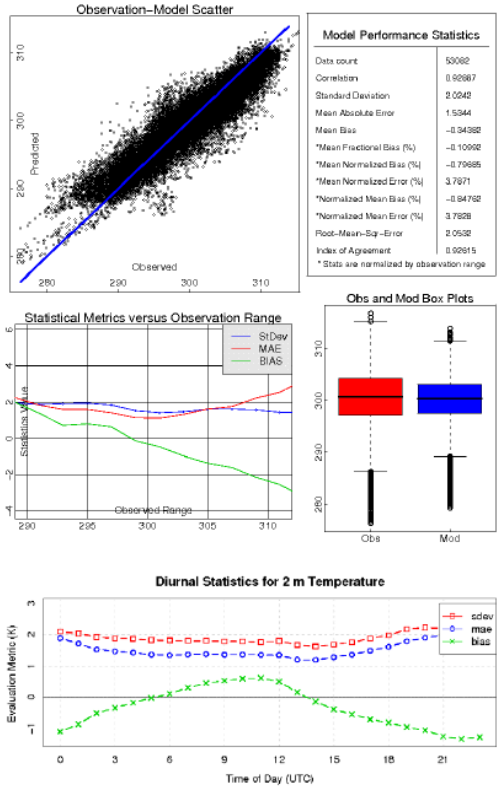

2-m WV Mix R

ACM2 – PX

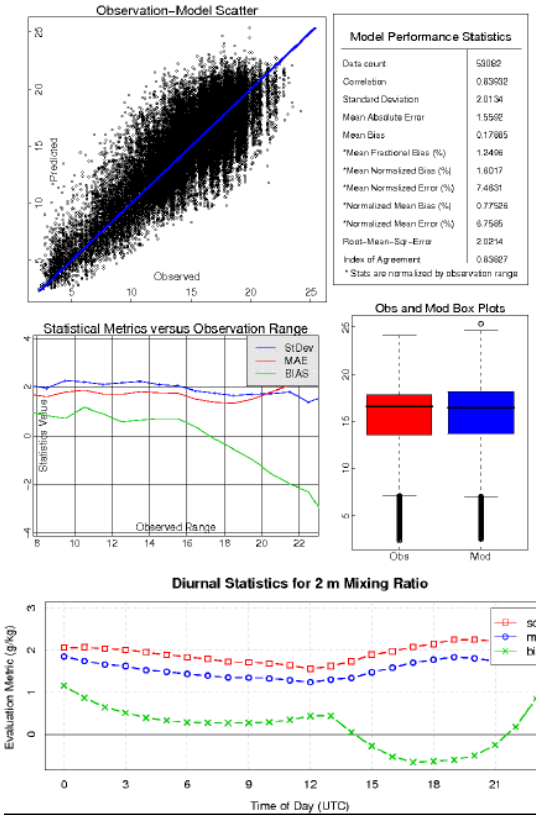

Blackadar – PX

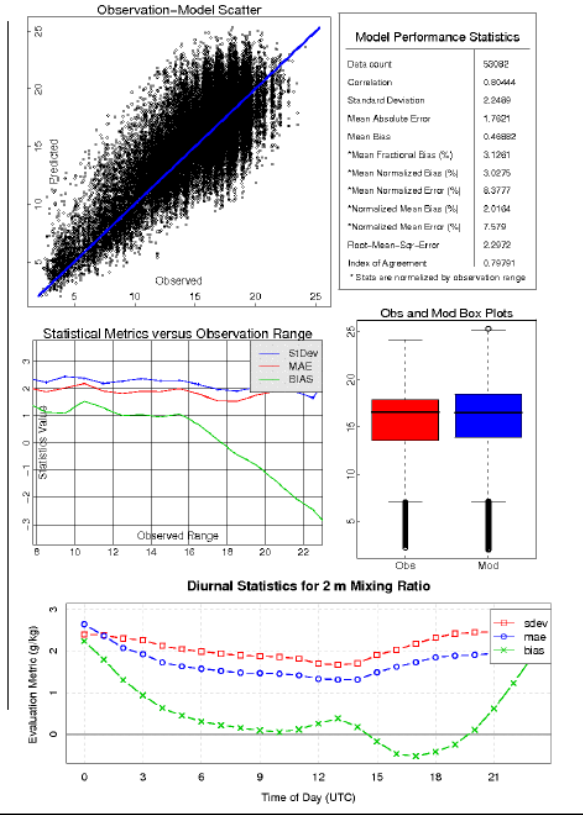

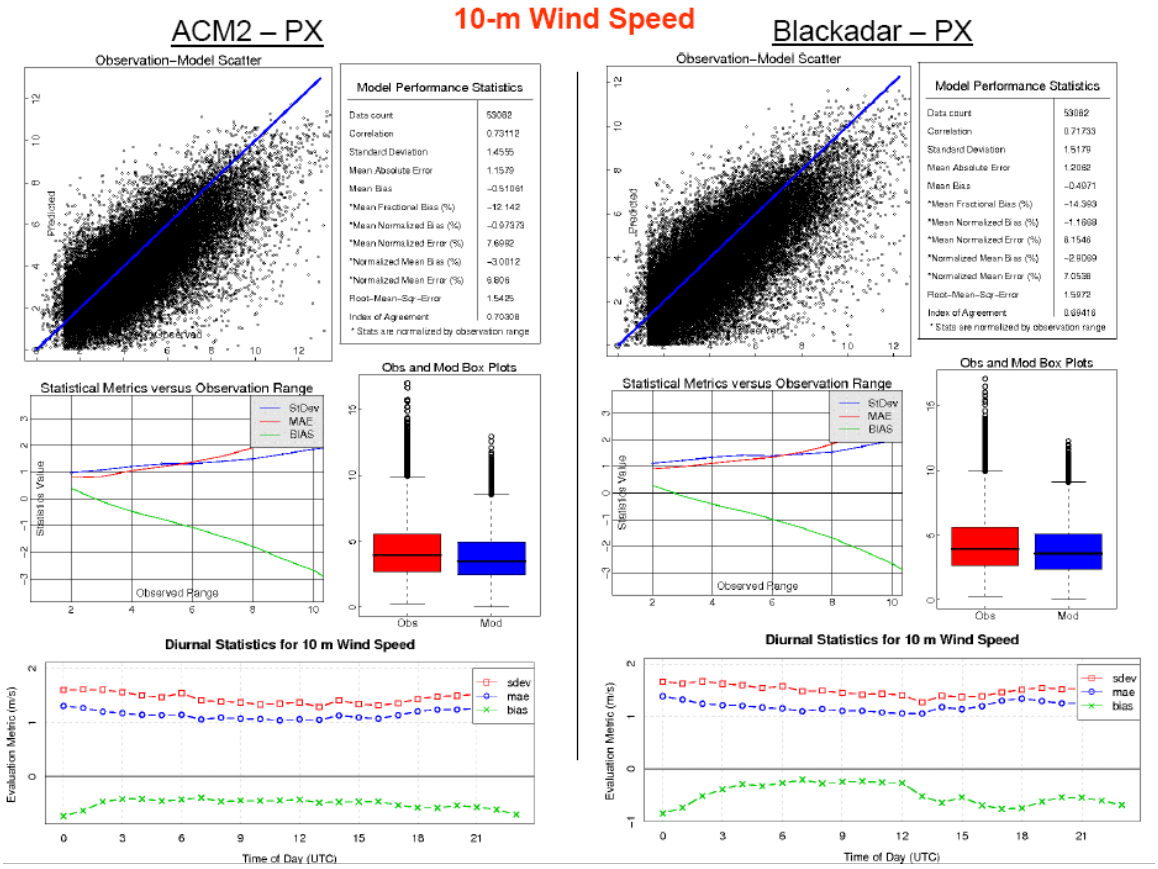

The EPA results show that ACM2(PX) and BLK perform similarly.

On December 9, the WRF Work Group determined that no PBL configuration stood out as optimal and that they each had weaknesses and strengths for different regions. Other researchers, such as *Borge et al*. (2008) and *Mao et al.* (2006), have also found no clear winner among the WRF PBL choices. At this point, the OTC had to make a decision on the model configuration to meet the schedule set for screening modeling. The other Regional groups that participated in the WRF Work Group decided to defer their decision on WRF settings for another month.

Looking at the sensitivity tests for the OTC region, both ACM2(PX) and BLK did well for 2 m temperature in summer and winter. For water vapor mixing ratio, ACM2(PX) and BLK had very similar performance. Winter humidity results were better with BLK in this category. Wind speed is important for ozone and $PM_{2.5}$ in both seasons primarily during the day when the concentrations are likely to be the highest. In this category, there was very little difference between ACM2(PX) and BLK. Precipitation, cloud cover, and vertical profile results were also comparable.

7.5 Configuration Comparison

One of the final tests was to examine the spatial distribution of the WRF simulation with the two PBL schemes – BLK and PXEPA. In this case, the results from

the summer episode are examined by comparing the simulated mixing ratio, temperature at 2m and wind speed with the TDL database. At each TDL location, based on the daily RMSE, the median value was determined for the two PBL schemes and the smaller of these medians is shown in the Figure below as 3-panels for temperature, wind speed and mixing ratio, respectively.

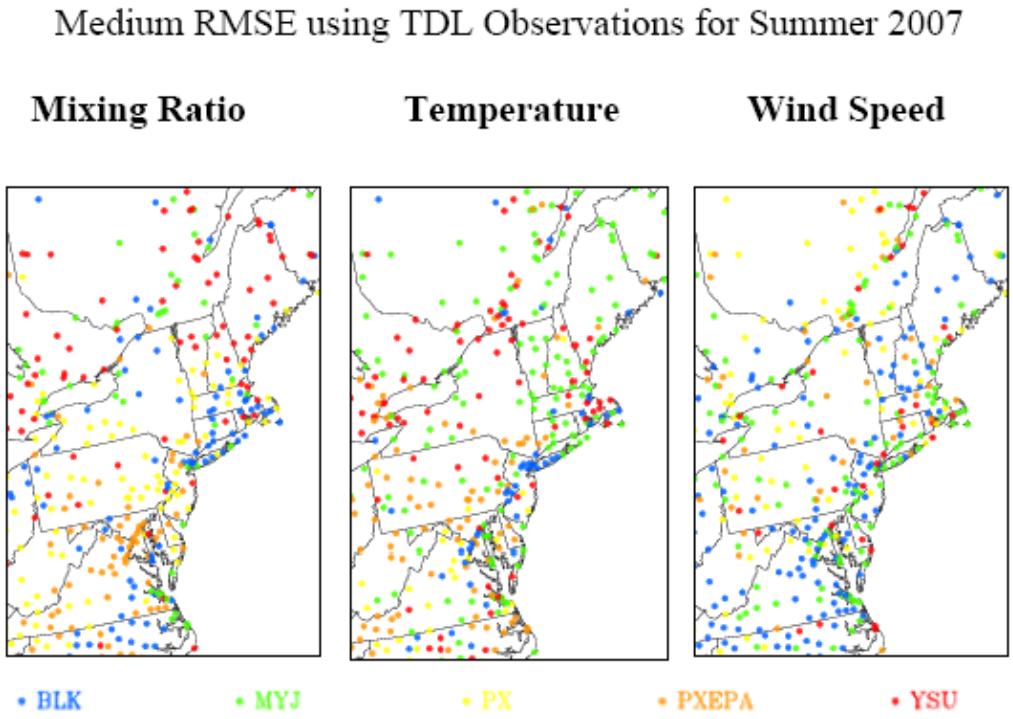

Based on 10-m wind speed RMSE, BLK has better performance in OTR, Based on 2-m temperature RMSE, there is no clear choice. But BLK has better performance along I-95 corridor. Based on 2-m mixing ratio RMSE, PXEPA has better performance over most of the OTR.

Another tie breaker for the OTC was based on their choice of UMD to produce the WRF meteorology runs for the SIPs. Prof. Da-Lin Zhang of UMD developed the BLK scheme for MM5 and used BLK in the OTC meteorology simulations for the 2002 SIPs. Given the familiarity these modelers had with BLK, troubleshooting any problems during the final production runs of WRF would go more smoothly than with the ACM2(PX) scheme. The other concern of using ACM2(PX) is that more than 10 days of model spin-up is recommended to let soil moisture reach saturated state to improve the performance. This would heavily increase the computing resource and the annual simulation needed to be run in sequential way (Gilliam and Pleim, 2010).

Another deciding factor was EPA's announcement that they were working on a 2007 WRF meteorology run with ACM2(PX) that they were going to make the results available to all regions. The choice of BLK gives the OTC and other regions the

flexibility to use a different WRF configuration for Weight of Evidence modeling. For all these reasons, OTC chose to use the BLK scheme to simulate boundary layer processes in WRF.

For *microphysics*, the OTC decided to go with WSM6 rather than WSM5, since WSM6 treats grapuel, and is less computer resource intensive than Morrison. *Borge et al.* (2008) found that WSM6 had the lowest bias error for temperature (0.05K) and lowest RMSE for wind speed (2.67 m s-1) compared to WSM5, Lin, and Eta microphysics schemes. The choice of microphysics schemes was highly influential on precipitation and, consequently, on wet deposition. Overall, WSM6 performed the best.

For *land model*, the OTC chose the Pleim-Xui land model (PX LSM) because it improved temperature and humidity performance in the summer and was compatible with the chosen surface layer scheme.

For *surface layer*, the Pleim-Xui surface layer scheme was chosen because it improved the performance of BLK and was compatible with the chosen land surface model. This scheme was also recommended by EPA.

For *radiation*, the Dudhia shortwave and RRTM longwave schemes were chosen. *Borge et al.* (2008) found that three longwave radiation schemes (RRTM, GFDL, and CAM) performed similarly in WRF sensitivity tests for air quality applications. They picked the MM5 (Dudhia) scheme as the best shortwave radiation scheme for temperature and wind direction compared to the Goddard scheme. *Baker & Dolwick* (2009) evaluated the Dudhia shortwave radiation parameterization in MM5 by making comparison with SURFAD (SURface RADiation Budget Network) and ISIS (Integrated Surface Irradiance Study) monitordata. They found that this scheme used did not show strong systematic bias on a monthly but had a slight underprediction in early morning and overprediction in the afternoon.

For *cumulus convection*, the Kain-Fritsch scheme was selected. No sensitivity testing was done in this category since the both UMD and EPA recommended the same parameterization.

Details of each parameterization selected are summarized in the next section.

8 Final Model Configuration and Production

In this section, the OTC WRF settings are summarized then the major parameterizations are described. All model settings are documented in the WRF namelist and the WRF Preprocessing System (WPS) namelist in Appendix B.

The time period for the WRF simulation is from December 31, 2006 to December 31, 2007, a full year of hourly meteorology fields for 2007 CMAQ simulations. The outer domain of the continental United States was produced with a 36-km horizontal resolution and an inner nest of the Northeastern United States, east of the Rockies was produced at 12-km resolution. Both the outer domain and inner nest had 35 levels.

The geographic data for the outer domain was at 10 m resolution and for the inner nest was 2 m resolution. The North American Mesoscale (NAM) model fields with 40 km horizontal resolution, 27 vertical levels, and 3-hour intervals were used for initial and boundary conditions. The map projection was Lambert conformal conic projection with the first true latitude of 33° N and second true latitude of 45°N with 97°W as the longitude parallel to the conic axis. The model was reinitialized after each segment of 5.5 days (132 hours).

A 90-second time step was used for both the outer domain and inner nest simulations. For parameterizations, the radiation time step was 15 minutes, cumulus time step was 5 minutes, and PBL/surface layer time step was 90 seconds.

The Advanced Research WRF (ARW) core was used in non-hydrostatic mode. No damping was applied to the dynamics. The turbulence and mixing algorithms were determined by the PBL scheme and the eddy coefficient was calculated using the horizontal Smagorinsky first order closure (both these options are recommended by NCAR for real data cases). No 6th order diffusion was used. Specified boundary conditions were used and these boundaries were relaxed over 5 points.

The WRF physics categories are: (1) planetary boundary layer, (2) surface layer, (3) land-surface model, (4) microphysics, (5) cumulus parameterization, (6) shortwave radiation, and (7) longwave radiation.

8.1 Modified Blackadar PBL Scheme

The modified Blackadar planetary boundary layer scheme has two modules. The first is for stable and nocturnal boundary layers based on K theory. The second is for unstable and free convection based on a convective plume model. This parameterization determines the K-coefficient by the Richardson number, where the critical Richardson number is set to be 0.25. In addition, the mixing length is set to be the thickness of the model layer rather than a constant 100 m. It also uses potential temperature rather than virtual potential temperature to calculate the bulk Richardson number, R_b. Mass exchange coefficients are applied not only to wind speeds but also to potential temperature and water vapor mixing ratio. More information on modified BLK is available in *Zhang and Zhang* (2004)

8.2 Pleim-Xiu Surface Layer Scheme

The Pleim-Xiu surface layer scheme, new in WRF 3.0, is an accurate and economical estimation of flux-profile relationships. It determines vertical eddy diffusivity is based on boundary layer scaling similarity theory. This eddy diffusion component is critical for realistic gradients in the surface layer. It is different from other surface layer schemes in that it includes parameterizations of a viscous sub-layer in the form of a quasi-laminar boundary layer resistance. This accounts for differences in the diffusivity of heat, water vapor, and trace chemical species. The surface layer similarity functions are estimated by analytical approximations from state variables. For very stable surface layers, it uses a reduced slope to avoid decoupling from the surface. More information on PXSLM is available in *Pleim* (2007).

We set the first vertical layer, which represents the surface layer in this parameterization, within the 4–50 m range recommended by *Pleim* (2007).

8.3 Pleim-Xiu Land Surface Model

The Pleim-Xiu land model, new in WRF Version 3.0, is a two-layer force-restore soil temperature and moisture model with vegetation and sub-grid tiling [*Skamarock et al.* 2009]. The top layer is taken to be 1 cm thick, and the lower layer is 99 cm. The PXLM features three pathways for moisture fluxes: evapotranspiration, soil evaporation, and evaporation from wet canopies. Evapotranspiration is controlled by bulk stomatal and aerodynamics resistance that is dependent on root zone soil moisture, photosynthetically active radiation, air temperature, and the relative humidity at the leaf surface. Grid aggregate vegetation and soil parameters are derived from fractional coverage of land use categories and soil texture types. It relies on snow coverage data from NAM. According to *Gilliam and Pleim* (2010), its performance problems over snow have been ameliorated by an updated volumetric heat capacity and a new fractional snow cover algorithm. For more information on PXLM, see *Xiu and Pleim* (2001).

8.4 WSM6 Microphysics

The WRF Single Moment 6 (WSM6) scheme includes water vapor, rain, snow, cloud ice, cloud water, and graupel processes. It represents mixed-phase particle fall speeds for the snow and graupel particles by assigning a single fall speed to both weighted by the mixing ratios. It applies this fall speed to both sedimentation and accretion processes. WSM6 is recommended for high-resolution simulations, considering its efficiency and theoretical background [*Skamarock et al.* 2009]. For more information, see *Hong and Lim* (2006).

8.5 Kain-Fritsch Cumulus Convection

The modified Kain-Fritsch (KF-Eta) cumulus convection parameterization uses a simple cloud model with moist updrafts and downdrafts, including the effects of detrainment, entrainment, and relatively simple microphysics [*Skamarock et al.* 2009]. A minimum entrainment rate is imposed to suppress widespread convection in marginally unstable but dry environments. The entrainment rate is varies as a function of low-level convergence.

The CAPE (convective available potential energy) removal time scale is used for closure. Shallow convection is allowed for any updraft that does not reach minimum cloud depth for precipitating clouds and this minimum depth varies as a function of cloud-base temperature. The entrainment rate is allowed to vary as a function of low-level convergence. For downdrafts, the source layer is the entire 150 – 200 mb deep layer just above cloud base, mass flux is specified as a fraction of updraft mass flux at cloud base, fraction is a function of source layer relative humidity, and detrainment is specified to occur in updraft source layer and below. For more information, see *Kain and Fritsch* (1990).

8.6 Dudhia Shortwave Radiation Scheme

The Dudhia shortwave radiation scheme has a simple downward integration of solar flux, accounting for clear-air scattering, water vapor absorption, and cloud albedo and absorption [*Skamarock et al.* 2009]. It uses look-up tables for clouds. This scheme was originally in MM5, but the WRF Version 3 scheme has an option to account for terrain slope and shadowing effects on the surface solar flux. Sloping and shadowing effects are turned on for the 2007 runs. For more information on this shortwave radiation scheme, see *Dudhia* (1989).

8.7 RRTM Longwave Radiation Scheme

The Rapid Radiative Transfer Model (RRTM) is a spectral-band scheme using the correlated-k method. It uses pre-set tables to accurately represent longwave processes due to water vapor, ozone, CO2, and trace gases (if present), as well as accounting for cloud optical depth [*Skamarock et al*. 2009] . RRTM is a reference broadband radiative transfer model that can accurately reproduce more resource-intensive line-by-line results. The molecular absorbers included are water vapor, carbon dioxide, ozone, methane, nitrous oxide, oxygen, nitrogen, and the halocarbons. It includes extinction from aerosols, clouds, and Rayleigh scattering. RRTM flux errors for a clear sky are below 1.0 W m^{-2} for all levels and its heating rates are within 0.1K d^{-1} in the troposphere, and within 0.3 K d^{-1} in the stratosphere [*Iacono et al*. 2008]. For more information on RRTM, see *Mlawer et al*. 1997.

8.8 WRF Output Fields

The WRF simulations with the final settings were run in January and February 2010. The hourly WRF outputs include three-dimensional fields of temperature, winds, pressure perturbations, moisture, water vapor mixing ratio, cloud water mixing ratio, rain water mixing ratio, ice water mixing ratio, snow water mixing ratio, radiation tendency, map-scale factors, longitude and latitude, Coriolis parameter, land use category, terrain height, PBL depth, accumulated convective/non-convective precipitation, surface sensible/latent heat flux, friction velocity, time-varying roughness length, surface emissivity, and albedo . A list of WRF output fields is provided in Appendix C.

References

Akylas, E., V. Kotroni, and K. Lagouvardos, 2006. Sensitivity of high-resolution operational weather forecasts to the choice of the planetary boundary layer scheme, *Atmos. Environ.*, 84, 49–57

Appel, K. W., S. J. Roselle, R. C. Gilliam, and J. E. Pleim, 2009. Sensitivity of the Community Multiscale Air Quality (CMAQ) Model v 4.7 results for the eastern United States to MM5 and WRF meteorological drivers, *Geosci. Model Dev. Discuss.*, 2, 1081–1114

Baker, K., and P. Dolwick, 2009. *Meteorological Modeling Performance Evaluation for the Annual 2005 Eastern U. S. 12-km Domain Simulation* (EPA 2/2/09)

Borge, R., V. Alexandrov, J. del Vas, J. Lumbreras, and E. Rodríquez, 2008. A comprehensive sensitivity analysis of the WRF model for air quality applications over the Iberian Peninsula, *Atmos. Environ.*, 42, 8560–8574

Dudhia, J., 1989. Numerical study of convection observed during the winter monsoon experiment using a mesoscale two-dimensional model, *J. Atmos. Sci.*, 46, 3077–3107

EPA 2007, *Guidance on the use of models and other analyses for demonstrating attainment of air quality goals for ozone, PM2.5 and Regional Haze*, EPA-454/B-07-002

De Meij, A., A. Gizella, C. Cuvelier, P. Thunis, B. Bessagnet, J. F. Vinuesa, L. Minut, and H. M. Kelder, 2009. The impact of MM5 and WRF meteorology over complex terrain on CHIMERE model calculations, *Atmos. Chem. Phys.*, 9, 6611–6632

Gilliam, R., and J. Pleim, 2010. Performance assessment of the Plein-Xiu LSM, Pleim surface-layer and ACM PBL Physics in version 3.0 of WRF-ARW (accepted by *Journal of Applied Meteorology and Climate*)

Gilliam, R., J. Pleim, and T. Otte, 2009. Multiscale meteorological modeling for air quality applications, EPA Atmospheric and Modeling Analysis Division Peer Review Conference, January 27–29, Research Triangle Park, NC

Gupta, S., R. McNider, M. Trainer, R. Zamora, K. Knupp, and M. Singh, 1997. Nocturnal wind structure and plume growth rates due to inertial oscillations, J. App. Meteor., 36, 1050–1063

Hong, S.-Y., and J.-O. Lim, The WRF single-moment six-class microphysics scheme, *J. Korean Meteor. S.*, 42, 129–151.

Iacono, M., J. Delamares, E. Mlawer, M. Shepard, S. Clough, and W. Collins, 2008. Radiative forcing by long-lived gases: Calculations with AER radiative transfer models, *J. Geophys. Res.*, 113, D13103, doi:10.1029/2008JD009944

Kain, J., and J. Fritsch, 1990. A one-dimensional entraining-detraining plume model and its application in convective parameterization, *J. Atmos. Sci.*, 47, 2784–2802

Lin, M., T. Holloway, T. Oki, D. G. Streets, and A. Richter, 2009. Multi-scale model analysis of boundary layer ozone over East Asia, *Atmos. Chem. Phys*. 9, 3277–3301.

Mao, Q., L. Gautney, T. Cook, M. Jacobs, S. Smith, and J. Kelsoe, 2006. Numerical experiments on MM5-CMAQ sensitivity to various PBL schemes, *Atmos. Environ*., 40, 3092–3110.

Mlawer, E., S. Taubman, P. Brown, M. Iacono, and S. Clough, 1997. Radiative transfer for inhomogeneous atmosphere: RRTM, a validated correlated-k model for the long wave. *J. Geophys. Res.*, 102, 16663–16682

Pleim, 2007. A combined local and nonlocal closure model for the atmospheric boundary layer, Part I: Model description and testing, *J. Appl. Meteor. Clim.*, 46, 1383–1395.

Skamarock, W., J. Klemp, J. Dudhia, D. Gill, D. Barker, M. Duda, X.-Y. Huang, W. Wang, and J. Powers, July 2008. *A description of the Advanced Research WRF Version* 3, NCAR Tech. Note, NCAR TN-475+STR, 113 pp.

Stauffer, D., N. Seaman, and F. Binkowski, 1991. Use of four-dimensional data assimilation in a limited-area mesoscale model. Part II: Effects of data assimilation within the planetary boundary layer. *Mon. Wea. Rev.*, 119, 734–754

Titove, M., A. Sturman, and P. Zawar-Reza, 2007. Improvement of predicted fine and total particulate matter (PM) component by applying several different chemical scenarios: A winter 2007 case study, *Sci. Total Environ.*, 385, 284–296.

Wang, W., C. Bruyère, M. Duda, J. Dudhia, D. Gill, H.-C. Lin, J. Michalakes, S. Rizvi, and X. Zhang, 2009. *Weather Research and Forecasting ARW Users Manual* (NCAR) 310 pp.

Xiu, A., and J. Pleim, 2001. Development of a Land Surface Model. Part I: Application in a Mesoscale Meteorological Model, *J. App. Meteor.*, 40, 192–209

Zhang, D.-L., and R. Anthes, 1982. A high resolution model of the planetary boundary layer: Sensitivity tests and comparison with SESAME-79 data, *J. App. Meteor.*, 21, 1594–1609

Zhang, D.-L., and W.-Z. Zhang, 2004. Diurnal cycles of surface winds and temperatures as simulated by five boundary layer parameterizations, *J. App. Meteor.*, 114, 157–169

Appendix A: State Implementation Plan Requirements

2008 & 2010 Ozone NAAQS		
Date	**Milestone**	**Comment**
3/12/08	NAAQS signed-Effective date: May 27, 2008 (75 ppb)	March 27, 2008 Federal Register, 73 FR 16436 http://www.epa.gov/fedrgstr/EPA-AIR/2008/March/Day-27/a5645.pdf
3/12/09	Governor's recommendations due (75 ppb)	Recommendations based on 06-07-08 ozone data. Section 107(d)(1)(A) requires states recommendations be made by the Governor for future nonattainment areas within 1 year of the standard promulgation.
1/6/10	EPA proposes new NAAQS for ozone (60–70 ppb)	The new 8-hour primary ozone standard is set within the range 60–70 ppb. A new cumulative seasonal secondary ozone standard is set within the range 7–15 ppm-hours.
3/12/10	EPA supposed to publish final area designations (75 ppb)	Final designations should be based on 07-08-09 data. Section 107(d)(1)(B) requires the designations to be made final 2 years after the promulgation of a NAAQS, unless more data is needed, in which case an extra year may be provided (3 years after promulgation of the NAAQS)
8/31/10	EPA will finalize the new NAAQS for ozone (60–70 ppb)	After reading and responding to public comments, EPA will choose an 8-hour and annual standard for ozone.
January 2011	Governor's recommendations due (60–70 ppb)	States make recommendations for areas to be designated attainment, nonattainment, or unclassifiable.
3/12/11	Infrastructure SIP due in final form to EPA (75 ppb)	Section 110(a)(1) requires this submittal be made 3 years after standard promulgations. Modeling was not required for this SIP in the previous submittal. It is unclear what will be required of states in future infrastructure SIP submittals.
July 2011	EPA to publish final area designations (60–70 ppb)	EPA final area designations become effective in August 2011.
3/12/13	For areas designated nonattainment, plans are due to EPA in final form (75 ppb)	Section 172(b) requires this submittal be made 3 years after the date of the nonattainment designation. Final modeling results for projection years, including control strategy runs are needed at a minimum 1 year in advance of this date **(3/12/12).**

2008 & 2010 Ozone NAAQS		
Date	**Milestone**	**Comment**
December 2013	For areas designated nonattainment, plans are due to EPA in final form (60–70 ppb)	State Implementation Plans (SIPs) must outline how states will reduce pollution to meet standard. States are required to meet the primary standards from 2014 to 2031 based on the severity of the problem,
March 2016	Expected attainment date for Moderate Ozone Nonattainment Areas (75 ppb)	Table 1 40 CFR 51.903 provides 6 years to attain for a moderate nonattainment area from effective date of the designations for the 1997 standard. Therefore, it's expected that the same CAA-based time line (originally for the 1 hour standard in Section 181(a)) will be used for the 2008 standard. Since attainment must be demonstrated using **a full ozone season** of projections, the attainment summer becomes that of **2015**.
March 2019	Expected attainment date for Serious ozone nonattainment areas. (75 ppb)	Table 1 40 CFR 51.903 provides 9 years to attain for a serious nonattainment area from effective date of the designations for the 1997 standard. Therefore, it's expected that the same CAA-based time line (originally for the 1 hour standard in Section 181(a)) will be used in the 2008 standard. Since attainment must be demonstrated using **a full ozone season** of projections, the attainment summer becomes that of **2018.**

2006 $PM_{2.5}$ NAAQS		
Date	**Milestone**	**Comment**
9/21/06	NAAQS signed-Effective date: 12/18/06	October 17, 2006 Federal Register 71 FR 61144
12/17/07	Governor's recommendations due	Recommendations based on 04-05-06 data. Section 107(d)(1)(A) requires state's recommendations be made by the Governor for future nonattainment areas within 1 year of the standard promulgation.
December, 2008	EPA supposed to publish final area designations – *not yet published – expected soon.*	Section 107(d)(1)(B) requires the designations to be made final 2 years after the promulgation of a NAAQS, unless more data is needed, in which case an extra year may be provided (3 years after promulgation of the NAAQS)

2006 $PM_{2.5}$ NAAQS		
Date	**Milestone**	**Comment**
September, 2009	Infrastructure SIP due in final form to EPA	Section 110(a)(1) requires this submittal be made 3 years after standard promulgations. Previous infrastructure SIP submittals did not require modeling. It is unclear what will be required for future infrastructure SIP submittals.
December, 2012	For areas designated nonattainment, plans are due to EPA in final form -- *assuming designations will be finalized in December 2009*	Section 172(b) requires this submittal be made 3 years after the date of the nonattainment designation. Final modeling results for projection years, including control strategy runs are needed at a minimum 1 year in advance of this date **(December 2011).**
December 2014	Expected attainment date – *assuming designations will be finalized in December 2009*	Section 172(a)(2) lists the attainment date to be, ".. the date by which attainment can be achieved as expeditiously as practicable, but no later than 5 years from the date such area was designated nonattainment under section 107(d)…" It's expected that the same CAA-based time line will be used for the 2006 standard. Since attainment must be demonstrated using **a full year of data** projections, the attainment year becomes that of **2013**.

Appendix B: WRF Namelists

WPS Namelist

```
&share
 wrf_core = 'ARW',
 max_dom = 2,
 start_date = '2007-06-02_12:00:00','2007-06-02_12:00:00',
 end_date   = '2007-06-08_00:00:00','2007-06-08_00:00:00',
 interval_seconds = 10800,
 io_form_geogrid = 2,
/

&geogrid
 parent_id         =   1,   1,
 parent_grid_ratio =   1,   3,
 i_parent_start    =   1,  66,
 j_parent_start    =   1,  18,
 e_we              = 165, 250,
 e_sn              = 129, 250,
 geog_data_res     = '10m','2m',
 dx = 36000,
 dy = 36000,
 map_proj = 'lambert',
 ref_lat   =  40.00,
 ref_lon   = -97.00,
 truelat1  =  33.0,
 truelat2  =  45.0,
 stand_lon = -97.0,
 geog_data_path = '/data/meso-a/zhulin/geog3.1.1'
/

&ungrib
 out_format = 'WPS',
 prefix = 'FILE',
/

&metgrid
 fg_name = 'FILE'
 io_form_metgrid = 2,
/
```

WRF Namelist

```
 &time_control
 run_days                            = 0,
 run_hours                           = 132,
 run_minutes                         = 0,
 run_seconds                         = 0,
 start_year                          = 2007, 2007, 2000,
 start_month                         = 06,   06,   01,
 start_day                           = 02,   02,   24,
 start_hour                          = 12,   12,   12,
 start_minute                        = 00,   00,   00,
 start_second                        = 00,   00,   00,
```

```
end_year                            = 2007, 2007, 2000,
end_month                           = 06,   06,   01,
end_day                             = 08,   08,   25,
end_hour                            = 00,   00,   12,
end_minute                          = 00,   00,   00,
end_second                          = 00,   00,   00,
interval_seconds                    = 10800
input_from_file                     = .true.,.true.,.true.,
history_interval                    = 60,  60,   60,
frames_per_outfile                  = 1,   1,    1000,
restart                             = .false.,
restart_interval                    = 1440,
auxinput1_inname                    = "metoa_em.d<domain>.<date>"
io_form_history                     = 2
io_form_restart                     = 2
io_form_input                       = 2
io_form_boundary                    = 2
debug_level                         = 0
/

&domains
time_step                           = 90,
time_step_fract_num                 = 0,
time_step_fract_den                 = 1,
max_dom                             = 2,
s_we                                = 1,     1,
e_we                                = 165,   250,    94,
s_sn                                = 1,     1,
e_sn                                = 129,   250,    91,
s_vert                              = 1,     1,
e_vert                              = 35,    35,     28,
p_top_requested                     = 5000,
num_metgrid_levels                  = 27,
num_metgrid_soil_levels             = 4,
eta_levels                          = 1.0000, 0.9974, 0.9940, 0.9900,
                                      0.9854, 0.9796, 0.9723, 0.9635,
                                      0.9528, 0.9401, 0.9252, 0.9079,
                                      0.8882, 0.8659, 0.8410, 0.8133,
                                      0.7828, 0.7494, 0.7133, 0.6742,
                                      0.6323, 0.5878, 0.5406, 0.4915,
                                      0.4409, 0.3895, 0.3379, 0.2871,
                                      0.2378, 0.1907, 0.1465, 0.1056,
                                      0.0682, 0.0332, 0.0000
dx                                  = 36000, 12000,  3333.33,
dy                                  = 36000, 12000,  3333.33,
grid_id                             = 1,     2,     3,
parent_id                           = 0,     1,     2,
i_parent_start                      = 1,     66,    30,
j_parent_start                      = 1,     18,    30,
parent_grid_ratio                   = 1,     3,     3,
parent_time_step_ratio              = 1,     3,     3,
feedback                            = 1,
smooth_option                       = 0
/

&physics
mp_physics                          = 6,     6,     3,
```

```
ra_lw_physics                       = 1,     1,     1,
ra_sw_physics                       = 1,     1,     1,
radt                                = 15,    15,    30,
sf_sfclay_physics                   = 7,     7,     1,
sf_surface_physics                  = 7,     7,     2,
bl_pbl_physics                      = 11,    11,    1,
bldt                                = 0,     0,     0,
cu_physics                          = 1,     1,     0,
cudt                                = 5,     5,     5,
isfflx                              = 1,
ifsnow                              = 1,
icloud                              = 1,
surface_input_source                = 1,
num_soil_layers                     = 2,
pxlsm_smois_init                    = 0,  0,
sf_urban_physics                    = 0,
maxiens                             = 1,
maxens                              = 3,
maxens2                             = 3,
maxens3                             = 16,
ensdim                              = 144,
slope_rad                           = 1,
topo_shading                        = 1,
shadlen                             = 25000.,
/

&fdda
grid_fdda                           = 1,  1
gfdda_inname                        = "wrffdda_d<domain>",
GFDDA_END_H                         = 1310, 1310,
gfdda_interval_m                    = 180, 180,
fgdt                                = 0,
if_no_pbl_nudging_uv                = 0,  0,
if_no_pbl_nudging_t                 = 1,  1,
if_no_pbl_nudging_q                 = 1,  1,
if_zfac_uv                          = 0,
k_zfac_uv                           = 0,
if_zfac_t                           = 0,
k_zfac_t                            = 0,
if_zfac_q                           = 0,
k_zfac_q                            = 0,
guv                                 = 5.0E-4,2.5E-4,
gt                                  = 5.0E-4,2.5E-4,
gq                                  = 1.E-5,1.E-5,
if_ramping                          = 0,
dtramp_min                          = 60.0,
io_form_gfdda                       = 2,
grid_sfdda                          = 1, 1
sgfdda_inname                       = "wrfsfdda_d<domain>",
sgfdda_interval_m                   = 180, 180,
sgfdda_end_h                        = 1310, 1310,
io_form_sgfdda                      = 2,
guv_sfc                             = 5.0E-4,2.5E-4,
gt_sfc                              = 0, 0,
gq_sfc                              = 0, 0,
rinblw                              = 250
/
```

```
&dynamics
w_damping                           = 0,
diff_opt                            = 1,
km_opt                              = 4,
diff_6th_opt                        = 0,      0,      0,
diff_6th_factor                     = 0.12,   0.12,   0.12,
base_temp                           = 290.
damp_opt                            = 0,
zdamp                               = 5000.,  5000.,  5000.,
dampcoef                            = 0.01,   0.01,   0.2
khdif                               = 0,      0,      0,
kvdif                               = 0,      0,      0,
non_hydrostatic                     = .true., .true., .true.,
moist_adv_opt                       = 1,      1,      1,
scalar_adv_opt                      = 1,      1,      1,
/

&bdy_control
spec_bdy_width                      = 5,
spec_zone                           = 1,
relax_zone                          = 4,
specified                           = .true., .false.,.false.,
nested                              = .false., .true., .true.,
/

&grib2
/

&namelist_quilt
nio_tasks_per_group = 0,
nio_groups = 1,
/
```

Appendix C: WRF Output Variable Descriptions

Variable Description	Abbreviation
2nd order extrapolation constant	CF1
2nd order extrapolation constant	CF2
2nd order extrapolation constant	CF3
Accumulated potential evaporation	POTEVP
Accumulated total cumulus precipitation	RAINC
Accumulated total grid scale graupel	GRAUPELNC
Accumulated total noncumulus precipitation	RAINNC
Accumulated total grid scale snow and ice	SNOWNC
Albedo	ALBEDO
Albedo background	ALBBCK
Bulk richardson number	BR
Canopy water	CANWAT
Coriolis cosine latitude term	E
Coriolis sine latitude term	F
dη values on full (w) levels	DNW
dη values on full (w) levels inverse	RDNW
dη values on half (mass) levels	DN
dη values on half (mass) levels inverse	RDN
Dry air mass in column base-state	MUB
Dry air mass in column perturbation	MU
Emissivity surface	EMISS
Energy surface residual (noah lsm)	NOAHRES
Eta values on full (w) levels	ZNW
Eta values on half (mass) levels	ZNU
Extrapolation constant first	CFN
Extrapolation constant second	CFN1
Friction velocity (u*) in similarity theory	UST
Geopotential height base-state	PHB
Geopotential height perturbation	PH
Heat flux at the surface upward (sensible)	HFX
Heat flux at the surface upward accumulated (sensible)	ACHFX
Heat flux at the surface latent	LH
Heat flux at the surface latent accumulated	ACLHF
Heat flux ground (sensible)	GRDFLX
Heat flux ground accumulated (sensible)	ACGRDFLX
Height of forcing input	Z_FORCE
Inverse x grid length	RDX
Inverse y grid length	RDY
Land mask (1=land, 0=water)	LANDMASK
Land sea (1=land, 0=water)	XLAND
Land use category (24 categories)	LU_INDEX
Land use fraction by category	LANDUSEF

Variable Description	Abbreviation
Lapse rate base state	TLP
Latitude (south is negative)	XLAT
Latitude, u point	XLAT_U
Latitude, v point	XLAT_V
Leaf area index	LAI
Local cosine of map rotation	COSALPHA
Local sine of map rotation	SINALPHA
Longitude, u point	XLONG_U
longitude, v point	XLONG_V
Map factor in x-direction maximum in domain	MAX_MSTFX
Map factor in y-direction maximum in domain	MAX_MSTFY
Map scale factor on mass grid	MAPFAC_M
Map scale factor on u grid	MAPFAC_U
Map scale factor on v grid	MAPFAC_V
Map scale factor on mass grid in x-direction	MAPFAC_MX
Map scale factor in x-direction maximum in domain	MAX_MSTFX
Map scale factor on u grid in x-direction	MAPFAC_UX
Map scale factor on v grid in x-direction	MAPFAC_VX
Map scale factor on v grid in x-direction inverse	MF_VX_INV
Map scale factor on mass grid in y-direction	MAPFAC_MY
Map scale factor on u grid in y-direction	MAPFAC_UY
Map scale factor on v grid in y-direction	MAPFAC_VY
Mixing ratio, cloud water	QCLOUD
Mixing ratio, graupel	QGRAUP
Mixing ratio, ice	QICE
Mixing ratio, rain water	QRAIN
Mixing ratio, snow	QSNOW
Mixing ratio, water vapor	QVAPOR
Mixing ratio, water vapor at 2 m	Q2
Mixing ratio, water vapor at 2 m from analysis	Q2OBS
Mixing ratio water vapor x-advection upstream	QV_UPSTREAM_X
Mixing ratio water vapor x-advection upstream tendency	QV_UPSTREAM_X_TEND
Mixing ratio water vapor y-advection upstream	QV_UPSTREAM_Y
Mixing ratio water vapor y-advection upstream tendency	QV_UPSTREAM_Y_TEND
Model top zeta	ZETATOP
Model top pressure	P_TOP
Moisture flux at the surface (upward)	QFX
Monin-obukhov length	RMOL
Nest position	NEST_POS
Orographic convexity	CON
Orographic direction asymmetry function	OA1
Orographic direction asymmetry function	OA2
Orographic direction asymmetry function	OA3

Variable Description	Abbreviation
Orographic direction asymmetry function	OA4
Orographic direction asymmetry function	OL1
Orographic direction asymmetry function	OL2
Orographic direction asymmetry function	OL3
Orographic direction asymmetry function	OL4
Orographic shadow height	HGT_SHAD
Orographic variance	VAR
Planetary boundary layer height	PBLH
Precipitation, fraction of frozen	SR
Precipitation, bucket for cumulus	I_RAINC
Precipitation, bucket for non-cumulus	I_RAINNC
Pressure base-state	PB
Pressure at mean sea level	P00
Pressure perturbation	P
Pressure surface	PSFC
Radiation cloud fraction	CLDFRA
Radiation longwave flux at ground surface downward	GLW
Radiation longwave at top of atmosphere upward	OLR
Radiation shortwave flux at ground surface downward	SWDOWN
Ratio of base mass flux of downdrafts to updrafts	EDT_OUT
Resistance aerodynamic	RA
Resistance surface	RS
Roughness length background	Z0
Roughness length (time-varying)	ZNT
Runoff surface	SFROFF
Runoff underground	UDROFF
Sea ice flag	SEAICE
Sea ice flag previous step	XICEM
Sea surface temperature	SST
Sea surface temperature skin	SSTSK
Snow coverage (1=snow cover, 0=no snow cover)	SNOWC
Snow density	RHOSN
Snow depth water equivalent	SNOW
Snow height (physical)	SNOWH
Snow phase change heat flux	SNOPCX
Soil category, dominant	ISLTYP
Soil layer center depth	ZS
Soil layer thickness	DZS
Soil moisture	SMOIS
Soil temperature, annual mean for deep soil	TSLB
Soil temperature at lower boundary	TMN
Soil temperature at bottom	SOILTB
Temperature, skin (surface/ground)	TSK
Temperature at 2 m	T2
Temperature at 2 m from analysis	T2OBS

Variable Description	Abbreviation
Temperature at which base state temperature turns constant	TISO
Temperature base state	T00
Temperature potential at 2 m	TH2
Temperature potential perturbation	T
Temperature potential x-advection upstream	TH_UPSTREAM_X
Temperature potential x-advection upstream tendency	TH_UPSTREAM_X_TEND
Temperature potential y-advection upstream	TH_UPSTREAM_Y
Temperature potential y-advection upstream tendency	TH_UPSTREAM_Y_TEND
Terrain height	HGT
Time: minutes since simulation start	XTIME
Time: number of time step (integer)	ITIMESTEP
Time weight constants for small steps (2)	RESM
Topography (0=original real, 1=modified by wrf)	SAVE_TOPO_FROM_REAL
Turbulent kinetic energy	TKE
Vegetation category, dominant	IVGTYP
Vegetation fraction	VEGFRA
Vegetation fraction for PXLM	VEGF_PX
Vertical stretching lower weight	FNP
Vertical stretching upper weight	FNM
Vertical velocity large-scale	W_SUBS
Vertical velocity large-scale tendency	W_SUBS_TEND
Water vapor mixing ratio x-advection upstream	QV_UPSTREAM_X
Water vapor mixing ratio x-advection upstream tendency	QV_UPSTREAM_X_TEND
Water vapor mixing ratio y-advection upstream	QV_UPSTREAM_Y
Water vapor mixing ratio y-advection upstream tendency	QV_UPSTREAM_Y_TEND
Wind x-component	U
Wind x-component at 10 m	U10
Wind x-component geostrophic	U_G
Wind x-component geostrophic tendency	U_G_TEND
Wind x-component x-advection upstream	U_UPSTREAM_X
Wind x-component x-advection upstream tendency	U_UPSTREAM_X_TEND
Wind x-component y-advection upstream	U_UPSTREAM_Y
Wind x-component y-advection upstream tendency	U_UPSTREAM_Y_TEND
Wind y-component	V
Wind y-component at 10 m	V10
Wind y-component geostrophic	V_G
Wind y-component geostrophic tendency	V_G_TEND
Wind y-component x-advection upstream	V_UPSTREAM_X

Variable Description	Abbreviation
Wind y-component x-advection upstream tendency	V_UPSTREAM_X_TEND
Wind y-component y-advection upstream	V_UPSTREAM_Y
Wind y-component y-advection upstream tendency	V_UPSTREAM_Y_TEND
Wind z-component	W